Generalized Morse Wavelets Parameter Selection and Transfer Learning for pavements transverse cracking detection.

Defense of the research proposal

M.Sc. Erick Axel Martinez Rios

Committee:

Dr. Luis Montesinos
Dr. Hector Perez Meana
Dr. Rogelio Bustamante Bello
Dr. Sergio Navarro Tuch

Tecnológico de Monterrey

Outline

1. Introduction
2. Literature Review
3. Research Question, Hypothesis, and Objectives
4. Methodology
5. Results and Discussion
6. Limitations
7. Conclusions

Introduction

The analysis of signals can be performed in **three general frameworks [1,2]**:

- Time-domain analysis: Focused on how the signal's amplitude changes with time.
- Frequency-domain analysis: Focused on the signal's spectral content obtained through the Fourier Transform.
- **Time-Frequency analysis:** Focused on the spectral content of the signals that change with time**.**

Introduction

Heisenberg Uncertainty principle: *It is not possible to arbitrarily concentrate a function in time and frequency simultaneously* [1,2].

- Time-Frequency Analysis
  - Short-Time Fourier Transform
  - Wavelet Transform

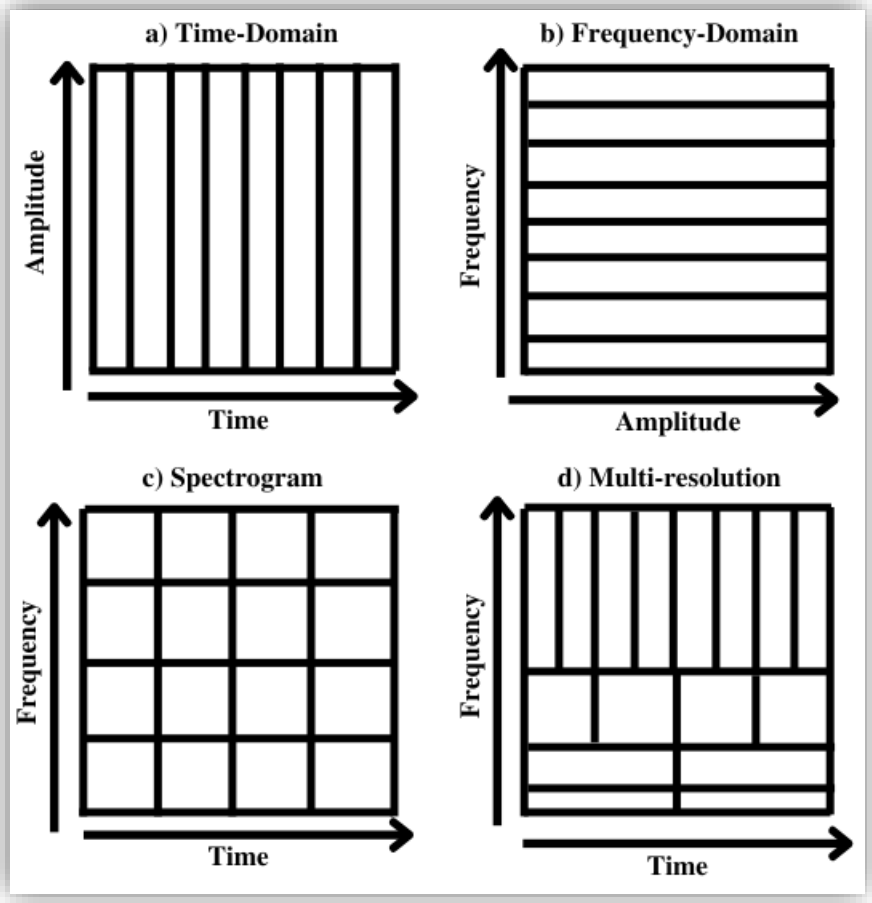

Figure 1. Comparison of signal representations and resolutions.

Signal representations and classification.

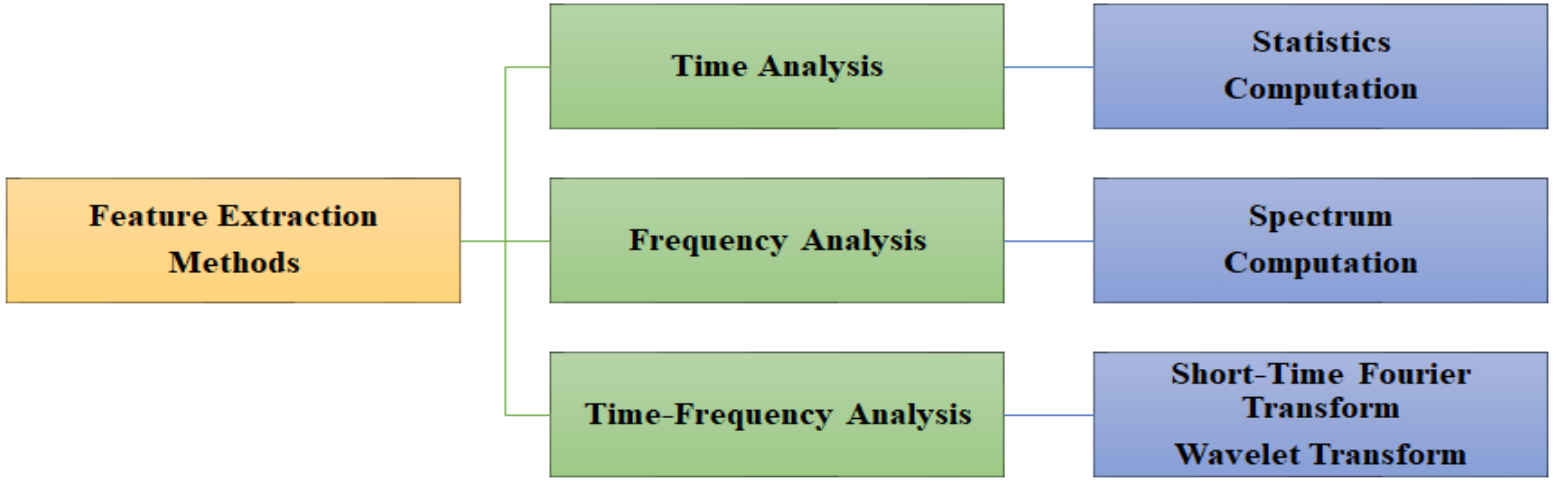

Figure 2. Overview of feature extraction methods based on signal representations[3,4].

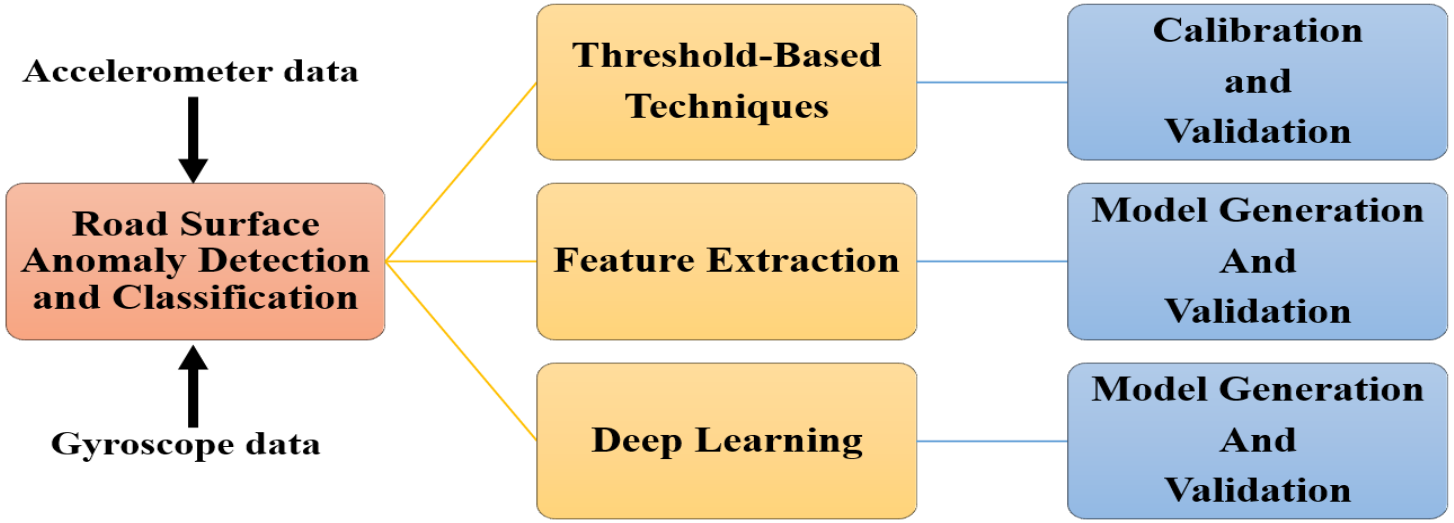

Figure 3. Overview of road surface anomaly detection and classification based on vibrations [3,4].

Tecnológico de Monterrey

Examples of studies related to road surface anomaly classification

Table 1. Examples of road surface anomaly classification and detection systems.

Author	Feature Extraction Methods	Anomaly	Algorithm	Performance
Sattar et al. [5]	**Threshold value**	Potholes Manholes Cracks Road joints	Hybrid approach Threshold plus Gaussian Mixture Model	Accuracy: 70%
Ferjani et al. [6]	**Time-domain Frequency-domain. Time-frequency domain.**	Potholes Metal bumps Asphalt bumps Worn out roads	**Decision Tree**	Accuracy: 94.00%
Wu et al. [7]	**Frequency domain and time-frequency domain.**	Pothole	**Random Forest**	Accuracy: 95.7%
Baldini et al. [9]	**Time-frequency domain.**	Potholes Cracks Transverse cracks Patches Rumble strips Speed bumps	**Convolutional Neural Network**	Accuracy: 97.20%
Luo et al. [8]	**Raw inertial sensor data.**	Pothole Bump Gravel Cobblestone Broken concrete	**Recurrent Neural Network**	Accuracy: 99.26%

Road anomaly classification and time-frequency analysis

Table 2. Examples of time-frequency methods employed in the literature [3].

Author	Method	Parameters
Baldini et al. [9]	**Short-Time Fourier Transform**	Window type, length, and overlap.
Li et al. [10]	**Continuous Wavelet Transform**	Daubechies 3 wavelet
Ferjani et al. [6]	**Discrete Wavelet Transform**	Daubechies 2 wavelet
Wu et al. [7]	**Discrete Wavelet Transform**	Reverse Biorthogonal Wavelet
Basavaraju et al. [11]	**Discrete Wavelet Transform**	Morlet wavelet

Tecnológico de Monterrey

Machine Learning algorithms **require a sizable sample size [23]**.

Collecting sufficient quality training data could be costly, challenging, and inefficient [23].

Setting the parameter **of Deep neural networks could be time-consuming and considered an art [23]**.

Machine Learning drawbacks.

Research Question

What are the properties of a mother wavelet that should be considered to generate a time-frequency representation for signal classification?

$$W f(u,s) = \langle\, f(t), \psi_{u,s}(t) \,\rangle = \int_{-\infty}^{\infty} f(t) \frac{1}{\sqrt{s}} \psi^*\left(\frac{t-u}{s}\right) dt$$

Stephane Mallat [12]

Hypothesis

- It is conjectured that **Generalized Morse Wavelets** could provide a basis to select an appropriate mother wavelet that helps to ***generate a time-frequency*** representation of vehicle vertical acceleration that can be used for pavement transverse cracking detection.

$$\Psi_{\beta,\gamma} = \int_{-\infty}^{\infty} \psi_{\beta,\gamma}(t) e^{-i\omega t} dt = U(\omega) a_{\beta,\gamma} \omega^{\beta} e^{-\omega^{\gamma}}$$

Lilly and Olhede [13]

Objectives

General Objective

To employ the wavelet transform through the GMWs to generate a time-frequency representation that can be used for pavement transverse cracking detection based on vehicle vertical acceleration signals.

Specific Objectives

- To define the gamma and beta values set of GMWs to create a time-frequency representation of the vehicle's vertical acceleration.
- To define a set of machine learning algorithms to process the time-frequency representations generated by GMWs.
- To train and validate a model based on machine learning that can detect pavement transverse cracking based on the scalogram of vehicle vertical acceleration data.

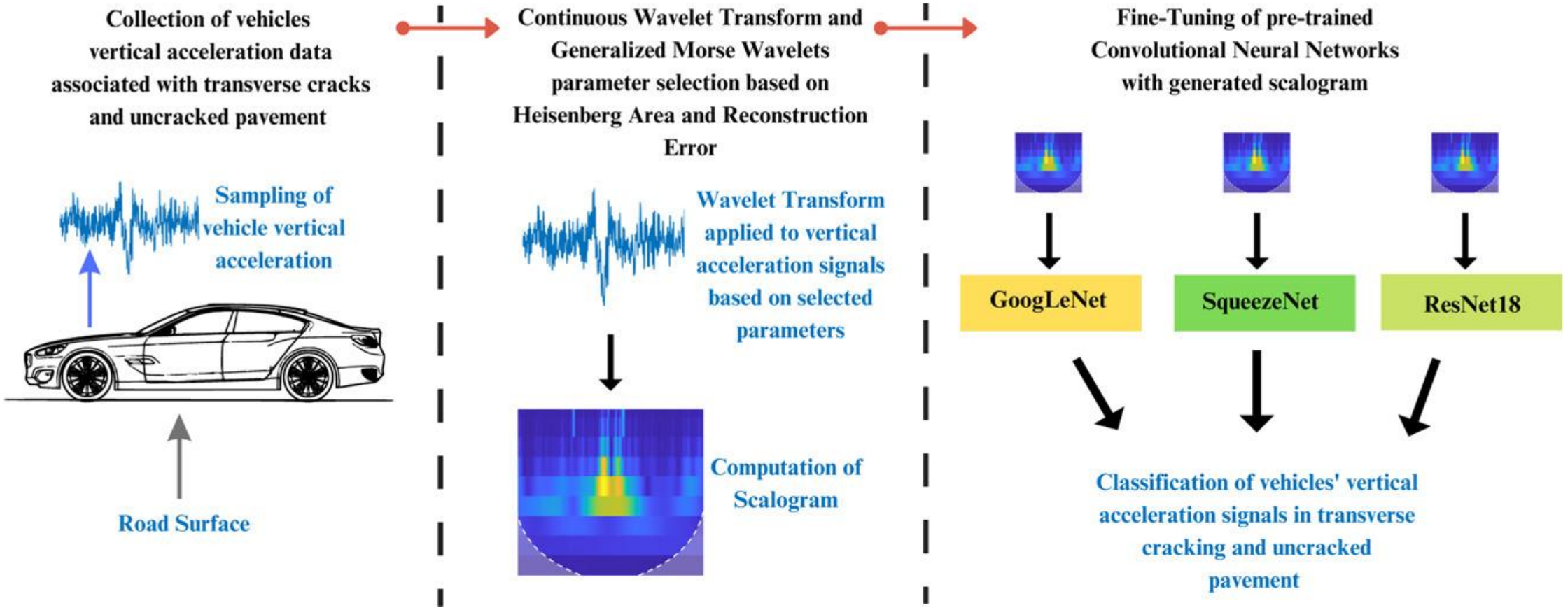

Figure 4. Overall methodology applied in this study [23].

Dataset

Yang, Q., Zhou, S.s., Wang, P., Zhang, J., 2021. **Application of signal processing and support vector machine to transverse cracking detection in asphalt pavement.** Journal of Central South University 28, 2451– 2462.

Dataset collected in Shangai, China.

Vehicle's vertical acceleration data associated with pavement transverse cracking.

The sensor was a piezoelectric analog accelerometer model CT100L.

The sampling frequency was set as 1280 Hz.

The sensor was placed in the front tire suspension knuckle.

The vehicle velocities were 30, 40, and 50 km/h.

The cracks had a width of 2 to 13 mm.

The sample size was of 327 signal segments.

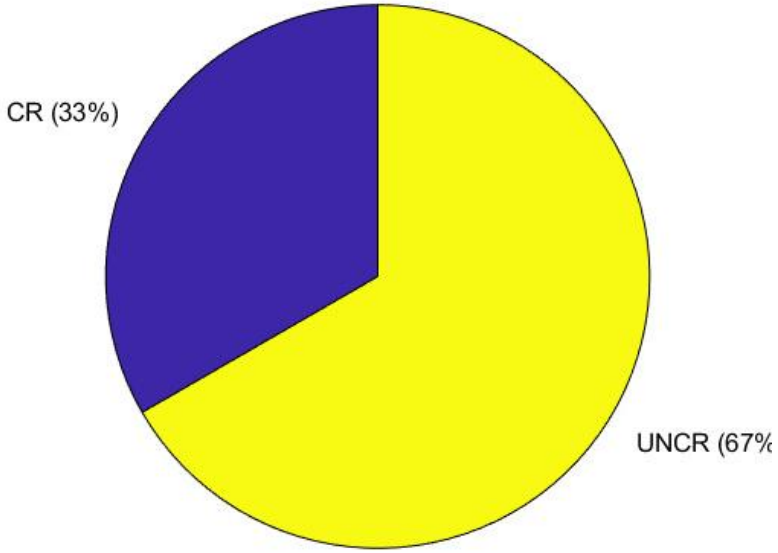

Figure 5. Distribution of the classes available in the dataset. CR: Cracked Sections. UNCR: Uncracked Sections [22].

General Methodology –

Selection of Gamma and Beta

- For $\gamma = 3$, generalized morse wavelets get near Heisenberg's area **lower-bound**.
- How to establish the **beta** parameter?

$$A_\psi \equiv \sigma_t \sigma_\omega \qquad \sigma_t \sigma_\omega \geq \frac{1}{2} \quad [12,13]$$

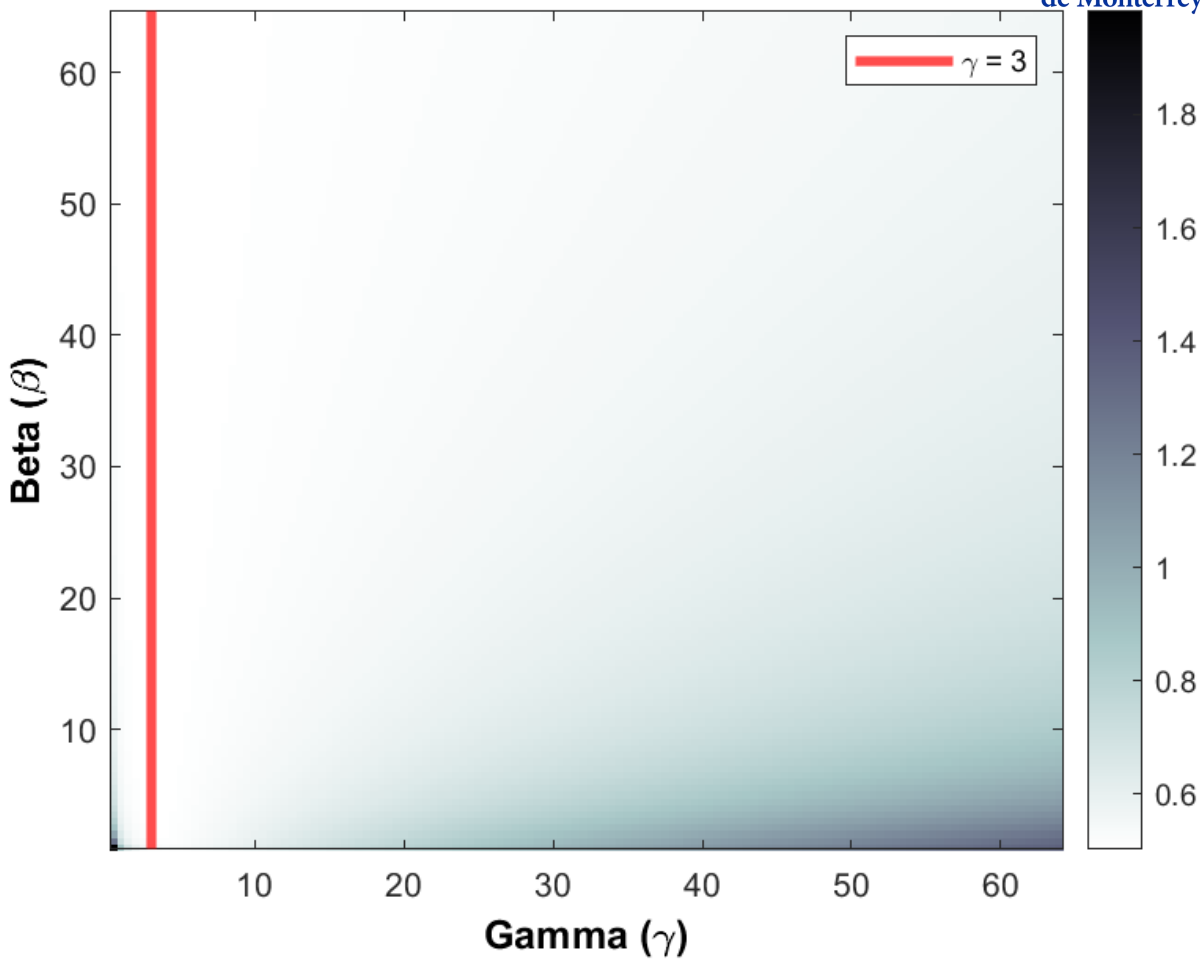

Figure 6. Heisenberg area of the generalized morse wavelets for different values of gamma and beta.

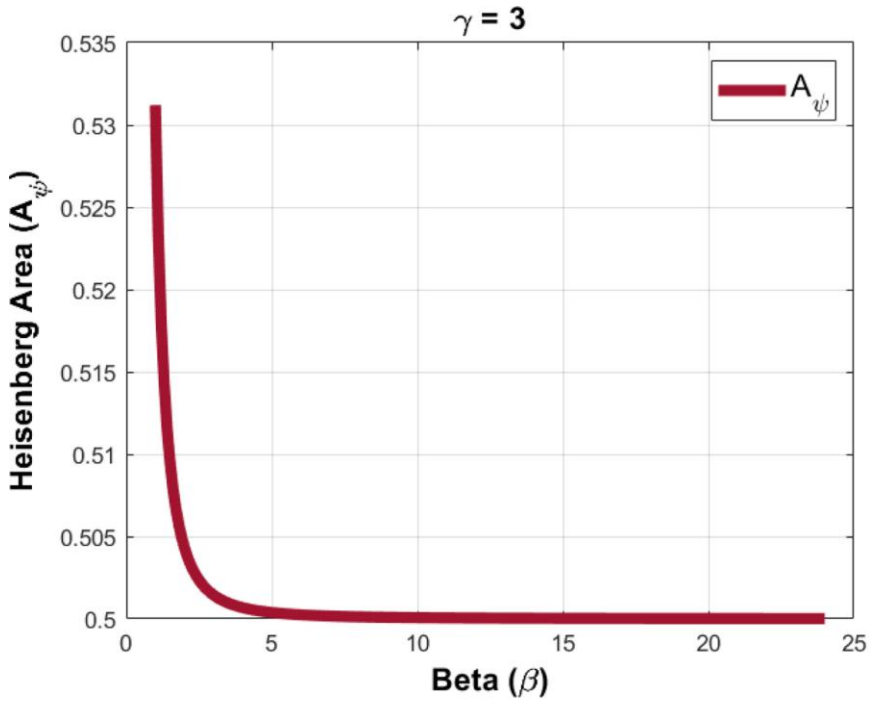

(a)

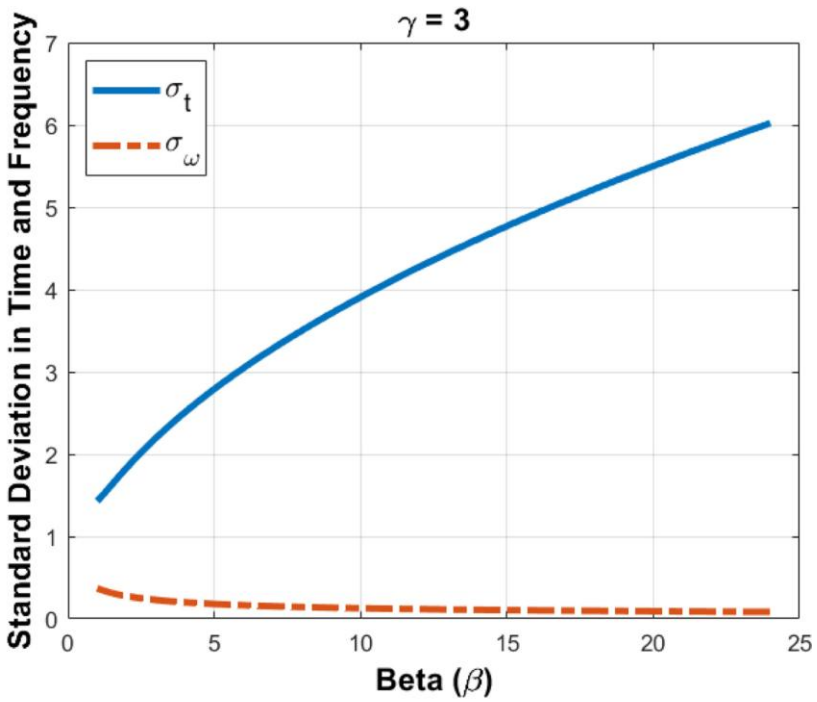

(b)

General Methodology –

Selection of Gamma and Beta

Figure 7. The behavior of the standard deviation in the time and frequency domain along with the Heisenberg Area for increasing values of beta and $\gamma = 3$ [23].

Proposed Methodology

Selection of **beta**.

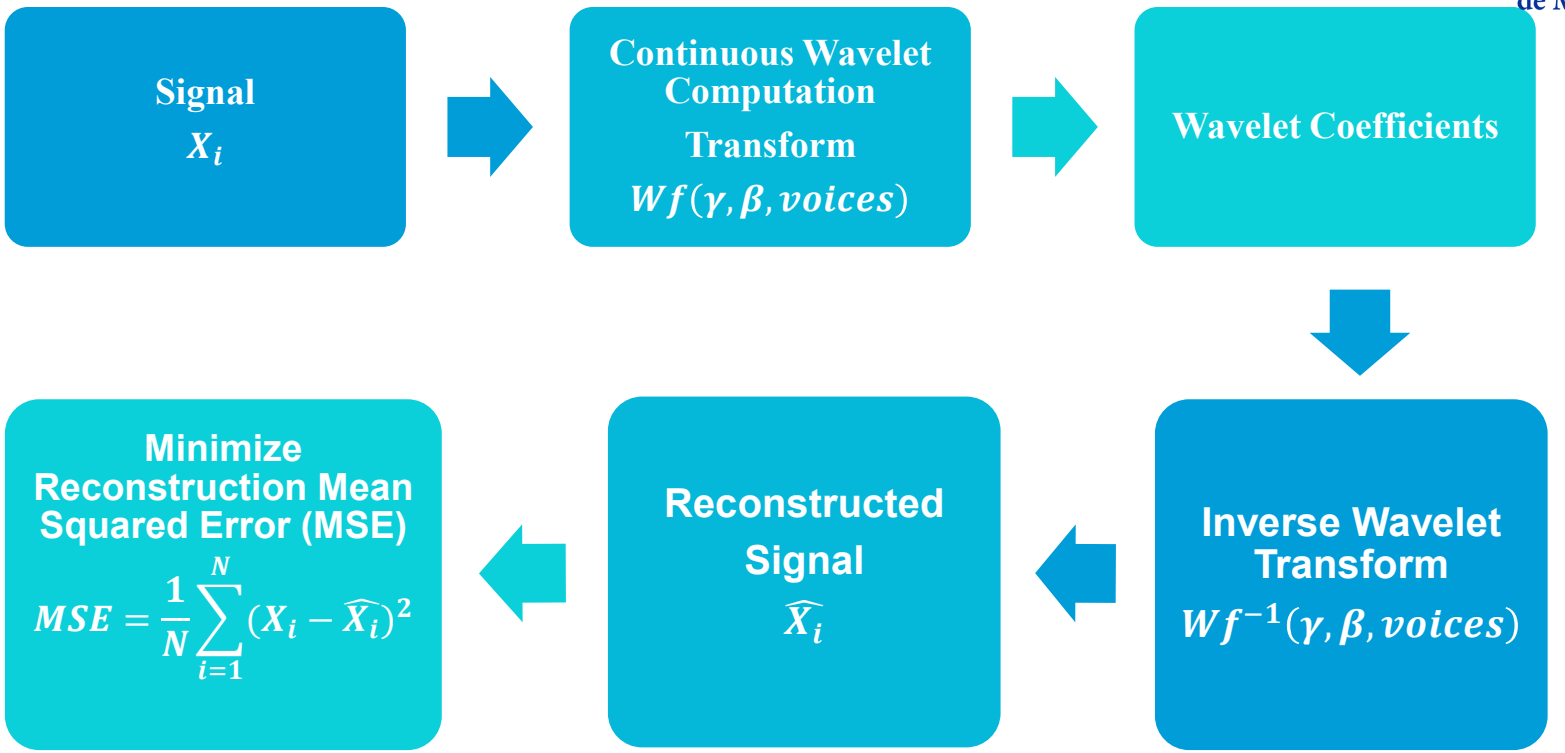

Average Reconstruction Mean Squared Error

- To consider the Reconstruction Mean Squared Error of each signal available in the dataset, the average of the error was computed as follows:

$$ARMSE = \frac{1}{N}\sum_{i=1}^{N} MSE_i$$

- Where $\boldsymbol{i}$ is an individual signal of the set of size $\boldsymbol{N}$and $\boldsymbol{MSE_i}$ is the individual reconstruction error of the signal $\boldsymbol{i}$.

Execution Environment:

- NVIDIA Graphics Processing Unit (GPU) GeForce GTX 1050 and 8.00 GB of RAM
- MATLAB 2022a

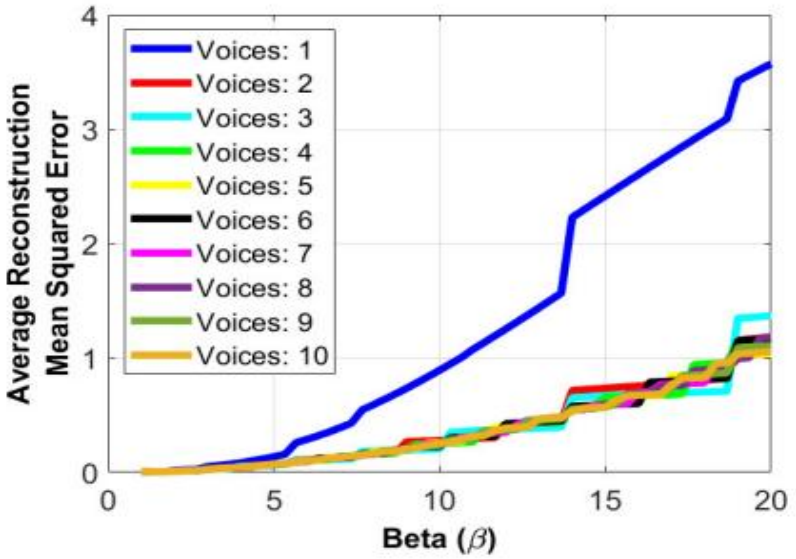

(a)

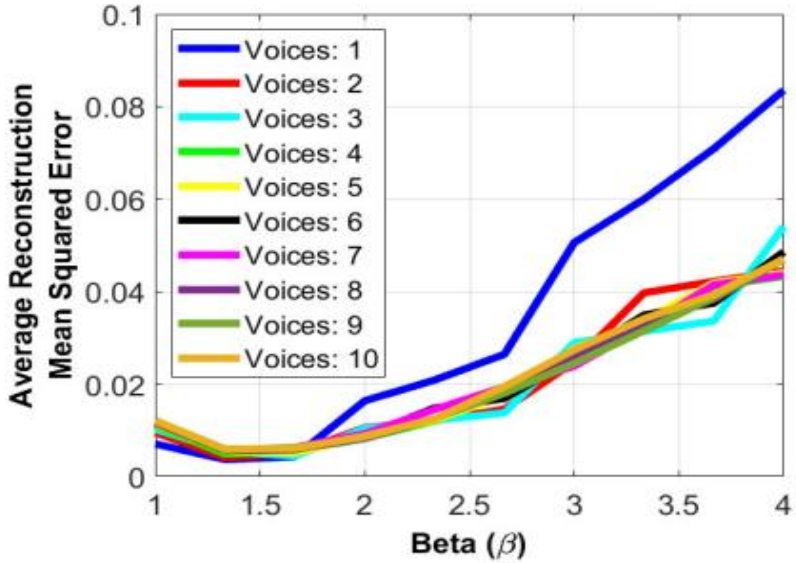

(b)

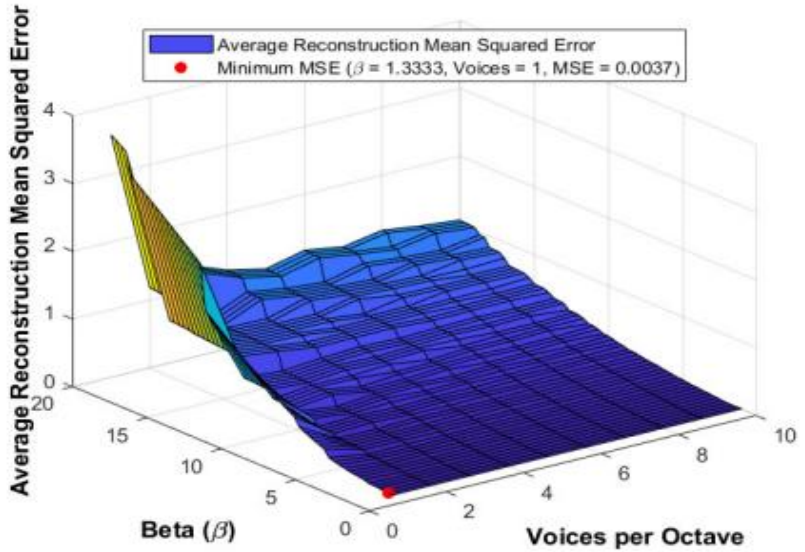

(c)

Figure 8. The behavior of the Average Reconstruction Mean Squared Error. The ARMSE was computed for integer values of the time-bandwidth product between 3 and 60. The number of voices per octave were set from 1 to 10 [23].

Voices = 1, $\beta = 1.3333$, $\gamma = 3$

Voices = 1, $\beta = 1.3333$, $\gamma = 3$

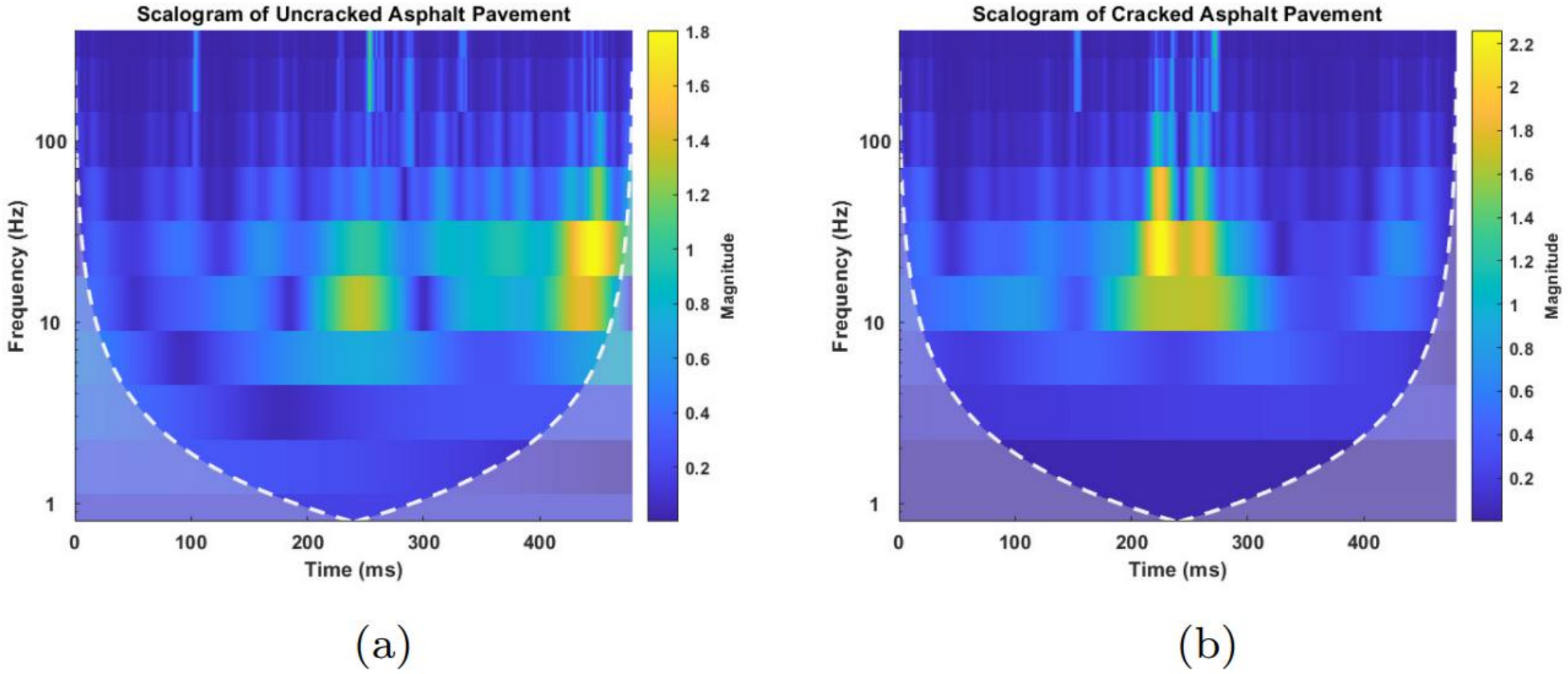

Figure 9. Scalogram of the vertical acceleration signals [23].

Fine-tuning of pre-trained CNNs

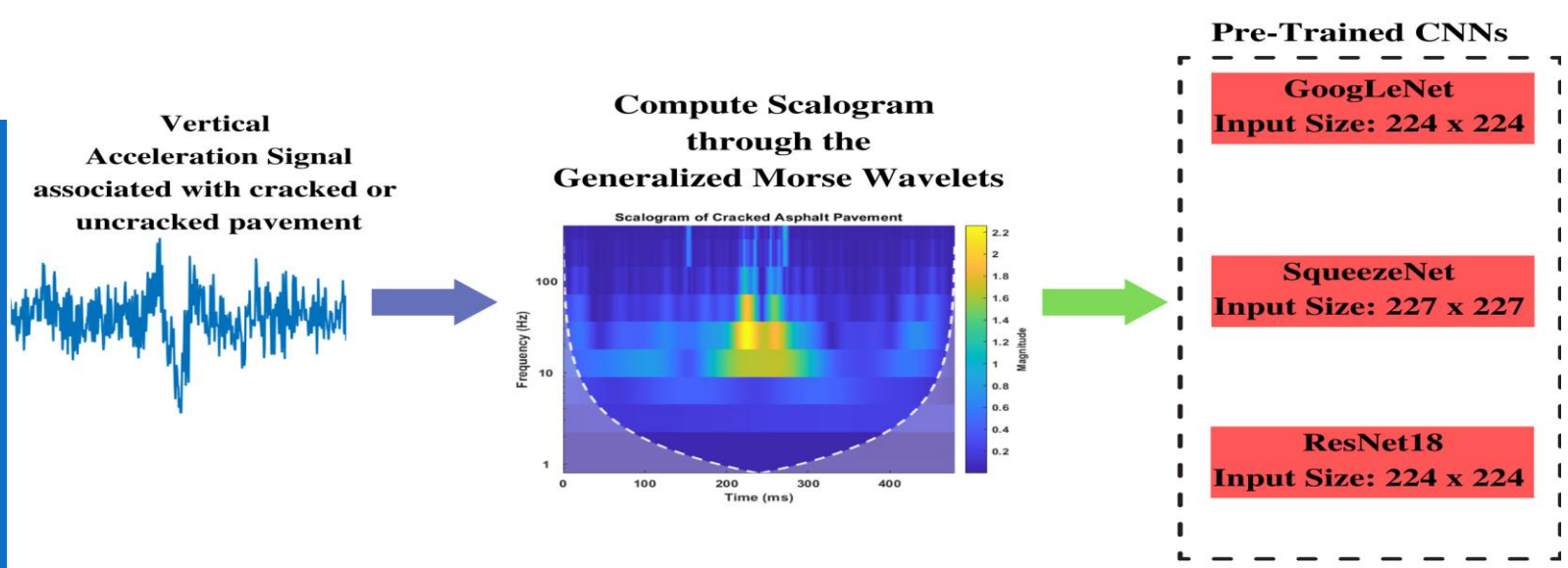

Figure 10. Methodology for fine-tuning the pre-trained CNNs [23].

Table 3. Characteristics of selected pre-trained CNNs [23].

CNN	Depth	Number of parameters (millions)
GoogLeNet	22	7.0
ResNet18	18	11.7
SqueezeNet	18	1.24

- Learning Rate: 0.0001
- Stochastic Gradient Descent
- Max Number of Epochs: 25
- Mini-batch size: 15

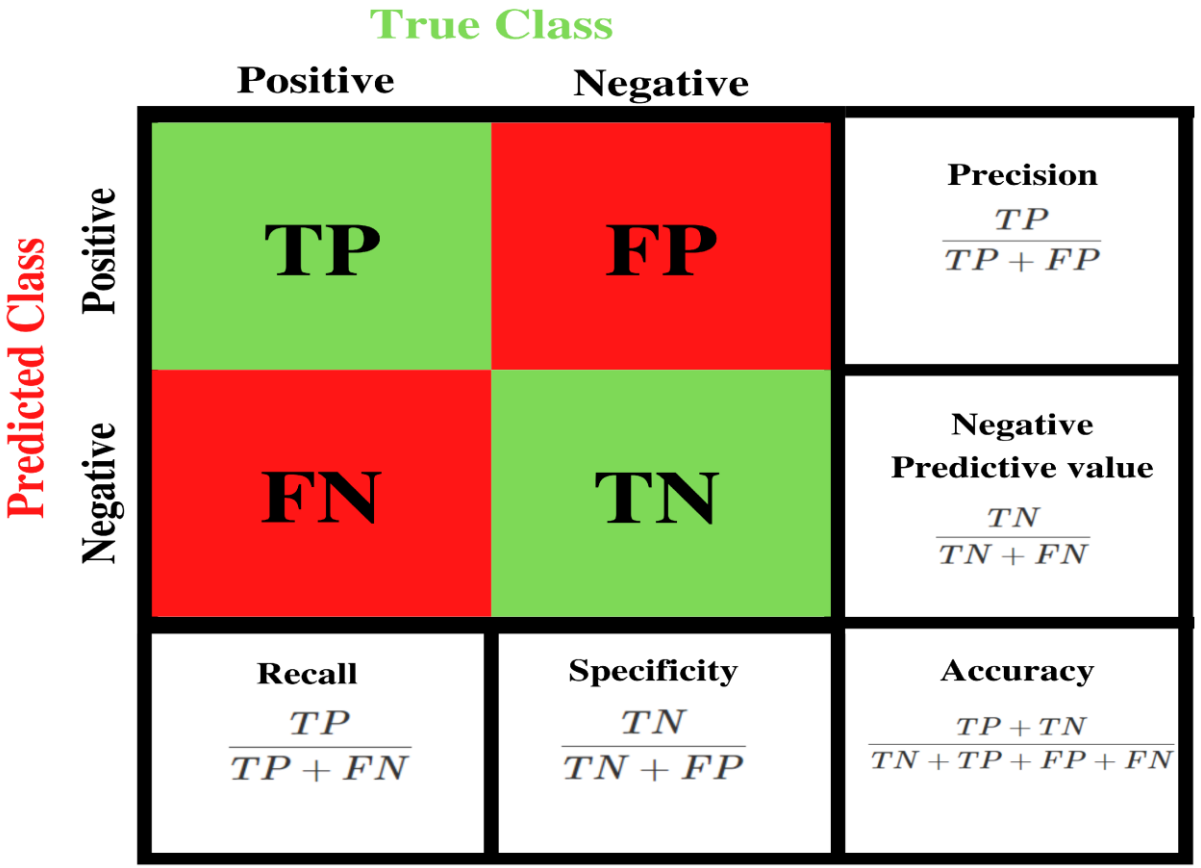

$$F1-Score=\frac{2(Recall)(Precision)}{Recall+Precision}$$

Evaluation Metrics

Figure 11. Confusion Matrix.

Tecnológico de Monterrey

Comparison with the literature

Table 4. 5-fold cross-validation results and Comparison with the literature [23].

Author	Features	Machine Learning Algorithm	Performance %
Yang et al. [22]	Time domain Frequency domain Wavelet domain	Support Vector Machine	Accuracy: 97.25 F1-score: 85.25
This study	Scalogram Computed with GMWs	GoogLeNet	Accuracy: 88.0886 ± 4.9536 Sensitivity: 76.9697 ± 8.9253 Specificity: 93.6047 ± 5.4074 F1-score: 81.1078 ± 7.5463
This study	Scalogram Computed with GMWs	SqueezeNet	Accuracy: 89.9301 ± 3.5959 **Sensitivity: 84.3290 ± 5.5704** **Specificity: 92.7061 ± 7.2403** **F1-score: 85.0201 ± 4.1592**
This study	Scalogram Computed with GMWs	ResNet18	Accuracy: 91.1422 ± 2.8848 Sensitivity: 77.9221 ± 5.3547 **Specificity: 97.7167 ± 2.7836** **F1-score: 85.3984 ± 4.7707**

Limitations of the study

- Limited sample size and unbalanced dataset.
- Only one vehicle type was used to collect the dataset.
- The training options of the pre-trained CNNs were fixed and not iterated.
- Only pavement transverse cracking was considered.
- The approach requires high-computational power and could be considered abstract in the case of CNNs.

Conclusions

- This work proposed using the **ARMSE** to set the beta parameter of GMWs and the number of voices per octave of the CWT for pavement transverse cracking detection.
- This process led to selecting a value of $\boldsymbol{\gamma = 3}$**, a** $\boldsymbol{\beta = 1.3333}$ **, and one voice per octave**.
- Moreover, transfer learning was used by **fine-tuning pre-trained CNNs such as SqueezeNet, GoogLeNet, and ResNet18** and employing the scalogram of the CWT as input.
- The 5-fold cross-validation results **showed that the SqueezeNet achieved a better performance than the ResNet18 and GoogLeNet** in terms of **sensitivity**.

Contributions

- The **Heisenberg area and the ARMSE** are used as reference metrics **to select the parameters of the GMWs** and the number of voices per octave of the CWT to generate a scalogram for pavement transverse cracking detection.

- Pre-trained CNNs such as **GoogLeNet, SqueezeNet, and ResNet18** are fine-tuned using 5-fold cross-validation to apply transfer learning **for pavement transverse cracking detection using the scalograms of vehicle's vertical acceleration signals as training data.**

applied sciences

MDPI

Review

A Review of Road Surface Anomaly Detection and Classification Systems Based on Vibration-Based Techniques

Erick Axel Martinez-Ríos *, Martin Rogelio Bustamante-Bello and Luis Alejandro Arce-Sáenz

Tecnologico de Monterrey, School of Engineering and Sciences, Mexico City 14380, Mexico
* Correspondence: a01331212@tec.mx

Abstract: Road surfaces suffer from sources of deterioration, such as weather conditions, constant usage, loads, and the age of the infrastructure. These sources of decay generate anomalies that could cause harm to vehicle users and pedestrians and also develop a high cost to repair the irregularities. These drawbacks have motivated the development of systems that automatically detect and classify road anomalies. This study presents a narrative review focused on road surface anomaly detection and classification based on vibration-based techniques. Three methodologies were surveyed: threshold-based methods, feature extraction techniques, and deep learning techniques. Furthermore, datasets, signals, preprocessing steps, and feature extraction techniques are also presented. The results of this review show that road surface anomaly detection and classification performed through vibration-based methods have achieved relatively high performance. However, there are challenges related to the reproduction and heterogeneity of the results that have been reported that are influenced by the limited testing conditions, sample size, and lack of publicly available datasets. Finally, there is potential to standardize the features computed through the time or frequency domains and evaluate and compare the diverse set of settings of time-frequency methods used for feature extraction and signal representation.

Keywords: road surface; anomaly classification; threshold; machine learning; deep learning; feature extraction

check for updates

Citation: Martinez-Ríos, E.A.; Bustamante-Bello, M.R.; Arce-Sáenz, L.A. A Review of Road Surface Anomaly Detection and Classification Systems Based on Vibration-Based Techniques. *Appl. Sci.* **2022**, *12*, 9413. https://doi.org/10.3390/app12199413

Academic Editors: Yuchuan Du and Yu Shen

Received: 7 September 2022
Accepted: 15 September 2022
Published: 20 September 2022

Publisher's Note: MDPI stays neutral with regard to jurisdictional claims in published maps and institutional affiliations.

1. Introduction

Road surface anomalies, such as potholes, cracks, rutting, or speed bumps deterioration, result from the constant usage, traffic loads, weather conditions, and age of the infrastructure and materials used in the construction of the roads [1,2]. These anomalies can be referred to as any deviation or variation from standard road conditions [3]. Furthermore, road defects have financial costs for governments to constantly maintain the road and keep it in good condition [4]. Moreover, it is crucial to attend to and monitor the road pavement condition due to the potential harm or accidents that could inflict on the vehicle users and pedestrians, its impact on fuel consumption, and the potential vehicle damage that these irregularities could inflict [5]. In addition, according to the World Bank, the density of paved roads in an optimal state can be used as an indicator of the economic strength and competitiveness of a country [6,7]. These factors make monitoring and maintaining the road in an optimal condition a crucial task for governments [8].

The traditional approach to monitoring and maintaining the road's optimal condition is to employ Pavement Condition Index (PCI) surveys that are based on human observations. These surveys have been used by international road and highway technicians as a reference to diagnose road anomalies [9]. The roughness of the road surface is another crucial indicator used to assess the quality of roads and detect cracks and bumps [10,11]. However, in the case of PCI surveys, they are prone to subjective evaluation by the technician and can put the health of road operators at risk [12]. Otherwise, visual inspection methods are time-consuming and prone to human errors [13]. Thus, to counter the disadvantages of

Tecnológico de Monterrey

Martinez-Ríos, E. A., Bustamante-Bello, M. R., & Arce-Sáenz, L. A. (2022). A Review of Road Surface Anomaly Detection and Classification Systems Based on Vibration-Based Techniques. *Applied Sciences*, *12*(19), 9413.

IEEE Access
Multidisciplinary | Rapid Review | Open Access Journal

Received 1 December 2022, accepted 26 December 2022, date of publication 27 December 2022, date of current version 3 January 2023.

Digital Object Identifier 10.1109/ACCESS.2022.3232729

TOPICAL REVIEW

Applications of the Generalized Morse Wavelets: A Review

ERICK AXEL MARTINEZ-RÍOS[1], ROGELIO BUSTAMANTE-BELLO[1], SERGIO NAVARRO-TUCH[1], (Member, IEEE), AND HECTOR PEREZ-MEANA[2], (Life Senior Member, IEEE)

[1]School of Engineering and Sciences, Tecnologico de Monterrey, Mexico City 14380, Mexico
[2]ESIME Culhuacan, Instituto Politecnico Nacional, Mexico City 04260, Mexico

Corresponding author: Erick Axel Martinez-Ríos (a01331212@tec.mx)

The work of Erick Axel Martinez-Ríos was supported by the Scholarship awarded by the Tecnologico de Monterrey and Consejo Nacional de Ciencia y Tecnologia through the Currículum Vitae Único (CVU) under Grant 1010770.

ABSTRACT The study of signals, processes, and systems has motivated the development of different representations that can be used to analyze and understand them. Classical ways of studying the behavior of signals are the time domain and frequency domain representations. For the analysis of non-stationary signals, time-frequency representations have become an essential tool to understand how the frequency content of signals changes with time. A common time-frequency technique employed in the literature is the wavelet transform. Nevertheless, selecting an adequate mother wavelet to perform the wavelet transform has become challenging due to the diverse available wavelet families. This paper reviews the applications and uses of a particular class of wavelet basis known as the Generalized Morse Wavelets. This class of wavelet family provides a systematic framework to choose and generate a wavelet for general-purpose use. This study reviews the application of Generalized Morse Wavelets in biomedical engineering, dynamical systems analysis, electrical engineering, geophysics, and communication systems. Moreover, the parameters of the Generalized Morse Wavelets used in each study are presented. The results of this study reveal that Generalized Morse Wavelets have proven helpful in studying signals, systems, and processes in areas ranging from biomedical engineering to geophysics. Nonetheless, the parameters of the Generalized Morse Wavelets are yet to be chosen through a rigorous methodology and argumentation. Therefore, there is an opportunity to generate methods for selecting the parameters of the Generalized Morse Wavelets based on the characteristics of the signals, systems, or processes under research.

INDEX TERMS Generalized Morse wavelets, mother wavelet selection, continuous wavelet transform, applications, time-frequency analysis.

Tecnológico de Monterrey

Martinez-Ríos, E. A., Bustamante-Bello, R., Navarro-Tuch, S., & Perez-Meana, H. (2022). Applications of the Generalized Morse Wavelets: A Review. IEEE Access.

Tecnológico de Monterrey

Martinez-Ríos, E. A., Bustamante-Bello, R., & Navarro-Tuch, S. A. (2023). Generalized Morse Wavelets parameter selection and transfer learning for pavement transverse cracking detection. Engineering Applications of Artificial Intelligence, 123, 106355.

Engineering Applications of Artificial Intelligence 123 (2023) 106355

Contents lists available at ScienceDirect

Engineering Applications of Artificial Intelligence

journal homepage: www.elsevier.com/locate/engappai

Generalized Morse Wavelets parameter selection and transfer learning for pavement transverse cracking detection

Erick Axel Martinez-Ríos *, Rogelio Bustamante-Bello, Sergio A. Navarro-Tuch

Tecnologico de Monterrey, School of Engineering and Sciences, Mexico City, 14380, Mexico

ARTICLE INFO

Keywords:
Continuous wavelet transform
Generalized Morse wavelets
Mother wavelet selection
Transfer learning
Convolutional neural networks
Pavement cracking detection

ABSTRACT

Monitoring road surface anomalies is crucial to avoid potential harm to pedestrians, vehicles, and vehicle users. These factors have motivated the development of systems that employ signal processing and machine learning algorithms to detect these irregularities automatically by sensing the vehicle's vibration. The wavelet transform (WT) has been frequently used for signal representation and feature extraction to solve signal classification problems. However, selecting a mother wavelet to perform the WT is challenging due to the need for methods that help to validate the time–frequency representation. Furthermore, machine learning algorithms require a sizeable sample size to train them, and setting their parameters is considered a time-consuming task. This paper proposes to compute the Continuous Wavelet Transform (CWT) through Generalized Morse Wavelets (GMWs) on vehicle's vertical acceleration data for pavement transverse cracking detection. The parameters gamma and beta of the GMWs and the CWT's voices per octave (VPO) were selected based on two metrics, the Heisenberg area and the Average Reconstruction Mean Squared Error. The scalogram generated through the CWT and GMWs was used to fine-tune pre-trained convolutional neural networks (CNNs) through transfer learning, such as GoogLeNet, SqueezeNet, and ResNet18. The proposed methodology set 1 VPO for the CWT, while the parameters gamma and beta of GMWs were set as 3 and 1.3333, respectively. The 5-fold cross-validation results of fine-tuning the CNNs showed that SqueezeNet provided a higher average validation sensitivity (84.3290 ± 5.5704) than GoogLeNet and ResNet18; however, the average validation specificity of SqueezeNet (92.7061 ± 7.2403) was lower.

1. Introduction

Maintaining the road infrastructure in an optimal condition is crucial to correct and prevent the possible degradation of the road surface (Lekshmipathy et al., 2021; Varona et al., 2020). Road surface anomalies can be a product of pavement age, weather conditions, traffic loads, and lack of maintenance (Martinez-Ríos et al., 2022). This degradation could include cracks, potholes, speed bumps deterioration, and grooves. In addition, these deviations present in the road surface could cause potential harm to vehicles, vehicle users, and pedestrians (Celaya-Padilla et al., 2018). Likewise, they can affect the energy consumption of automobiles. Furthermore, the maintenance of roads has financial costs for the government to repair these irregularities (Martinez-Ríos et al., 2022). The traditional approach in which the road's surface is monitored is through human observation performed by employing Pavement Condition Index Surveys (PCI) (ASTM, 2023). However, these surveys are prone to human errors and risk the health of road technicians (Martinelli et al., 2022; Shaghlil and Khalafallah, 2018; Yang and Zhou, 2021). The above factors have motivated the development of alternative methods to automatically detect and classify these road defects.

In this regard, recent studies have proposed using classification techniques based on signal processing and machine learning algorithms to detect or classify these anomalies by sensing the vehicle's vibration or through image processing and computer vision techniques (Sattar et al., 2021; Kim et al., 2022). For example, vibration-based methods detect and classify road surface anomalies by sensing the vehicle's vertical acceleration while it passes over the anomaly with the help of accelerometers (Sattar et al., 2018). Vibration-based structural damage has been developed since structural damage can change the dynamical characteristics of structures, such as natural frequencies, mode shapes, and damping ratios (Yang and Zhou, 2021). This approach has gained interest due to its cost-effectiveness, the low computational power needed to process accelerometer data, and potential real-time execution.

A typical strategy of vibration-based methods for road surface anomaly detection and classification is to employ classical signal processing techniques to extract features or statistics from a fixed time window of the vibration signal by considering different signal representations. These signal representations typically include the time

* Corresponding author.
E-mail addresses: A01331212@tec.mx (E.A. Martinez-Ríos), rbustama@tec.mx (R. Bustamante-Bello), snavarro.tuch@tec.mx (S.A. Navarro-Tuch).

https://doi.org/10.1016/j.engappai.2023.106355
Received 13 February 2023; Received in revised form 18 April 2023; Accepted 19 April 2023
Available online xxxx
0952-1976/

Overall Scientific Production

Tecnológico de Monterrey

Journal Articles

- **Martinez-Ríos, E. A.,** Bustamante-Bello, R., & Navarro-Tuch, S. A. (2023). Generalized Morse Wavelets parameter selection and transfer learning for pavement transverse cracking detection. Engineering Applications of Artificial Intelligence, 123, 106355.
- **Martinez-Ríos, E.A.,** R. Bustamante-Bello, S. Navarro-Tuch and H. Perez-Meana, "Applications of the Generalized Morse Wavelets: A Review," in IEEE Access, vol. 11, pp. 667-688, 2023, doi: 10.1109/ACCESS.2022.3232729.
- **Martinez-Ríos, E**. A., Bustamante-Bello, M. R., & Arce-Sáenz, L. A. (2022). A Review of Road Surface Anomaly Detection and Classification Systems Based on Vibration-Based Techniques. *Applied Sciences*, *12*(19), 9413.
- **Martinez-Ríos, E**., Ponce-Cruz, P. & Molina, A. A holistic educational platform for the study of the smart grid. Int J Interact Des Manuf 16, 841–861 (2022). https://doi.org/10.1007/s12008-022-00970-6
- **Martinez-Ríos, E.,** Montesinos, L., & Alfaro-Ponce, M. (2022). A machine learning approach for hypertension detection based on photoplethysmography and clinical data. *Computers in Biology and Medicine*, *145*, 105479.
- **Martinez-Ríos, E.,** Montesinos, L., Alfaro-Ponce, M., & Pecchia, L. (2021). A review of machine learning in hypertension detection and blood pressure estimation based on clinical and physiological data. *Biomedical Signal Processing and Control*, *68*, 102813.

Conference Articles

- **Martinez-Ríos, E.,** Montesinos, L., & Alfaro-Ponce, M. (2022). A Comparison Between Wavelet Scattering Transform and Transfer Learning for Elevated Blood Pressure Detection. BMEiCON2022.

Future Work

- Compare other time-frequency or wavelet-related techniques for pavement transverse cracking detection with the method presented in this study.

- **Short-Time Fourier Transform**

- **Hilbert-Huang Transform**

Gantt Diagram of Activities per Semester								
Activity	1	2	3	4	5	6	7	8
Literature Review								
First Publication								
Study of the Morse Wavelets								
Second Publication								
Dataset Selection								
Minimization of the reconstruction error for parameter selection.								
Classification algorithms selection or design								
Training of the algorithms and cross-validation simulation								
Third Publication								
Fourth Publication								
Thesis Development								

Tecnológico de Monterrey

References

[1] Franz Hlawatsch and François Auger. Time-frequency analysis. John Wiley & Sons, 2013.

[2] Steven L Brunton and J Nathan Kutz. Data-driven science and engineering: Machine learning, dynamical systems, and control. Cambridge University Press, 2022.

[3] Martinez-Ríos, E. A., Bustamante-Bello, M. R., & Arce-Sáenz, L. A. (2022). A Review of Road Surface Anomaly Detection and Classification Systems Based on Vibration-Based Techniques. *Applied Sciences*, *12*(19), 9413.

[4] Kim, Y. M., Kim, Y. G., Son, S. Y., Lim, S. Y., Choi, B. Y., & Choi, D. H. (2022). Review of Recent Automated Pothole-Detection Methods. *Applied Sciences*, *12*(11), 5320.

[5] Sattar, S.; Li, S.; Chapman, M. Developing a near real-time road surface anomaly detection approach for road surface monitoring. Measurement 2021, 185, 109990.

[6] Ferjani, I.; Alsaif, S.A. How to get best predictions for road monitoring using machine learning techniques. PeerJ Comput. Sci. 2022, 8, e941.

[7] Wu, C.; Wang, Z.; Hu, S.; Lepine, J.; Na, X.; Ainalis, D.; Stettler, M. An automated machine-learning approach for road pothole detection using smartphone sensor data. Sensors 2020, 20, 5564.

[8] Luo, D.; Lu, J.; Guo, G. Road anomaly detection through deep learning approaches. IEEE Access 2020, 8, 117390–117404.

[9] Baldini, G.; Giuliani, R.; Geib, F. On the Application of Time Frequency Convolutional Neural Networks to Road Anomalies' Identification with Accelerometers and Gyroscopes. *Sensors* **2020**, *20*, 6425.

[10] Li, X.; Huo, D.; Goldberg, D.W.; Chu, T.; Yin, Z.; Hammond, T. Embracing crowdsensing: An enhanced mobile sensing solution for road anomaly detection. *ISPRS Int. J. Geo-Inf.* **2019**, *8*, 412.

[11] Basavaraju, A.; Du, J.; Zhou, F.; Ji, J. A machine learning approach to road surface anomaly assessment using smartphone sensors. *IEEE Sensors J.* **2019**, *20*, 2635–2647.

[12] Stéphane Mallat. A wavelet tour of signal processing. Elsevier, 1999.

[13] Jonathan M Lilly and Sofia C Olhede. Generalized morse wavelets as a Superfamily of analytic wavelets. IEEE Transactions on Signal Processing, 60(11):6036–6041, 2012.

[14] Mark P Wachowiak, Renata Wachowiak-Smolíková, Michel J Johnson, Dean C Hay, Kevin E Power, and F Michael Williams-Bell. Quantitative feature analysis of continuous analytic wavelet transforms of electrocardiography and electromyography. Philosophical Transactions of the Royal Society A: Mathematical, Physical and Engineering Sciences, 376(2126):20170250, 2018.

Tecnológico de Monterrey

References

[15]Cartas-Rosado, R., Becerra-Luna, B., Martínez-Memije, R., Infante-Vazquez, O., Lerma, C., Pérez-Grovas, H., & Rodríguez-Chagolla, J. M. (2020). Continuous wavelet transform based processing for estimating the power spectrum content of heart rate variability during hemodiafiltration. Biomedical Signal Processing and Control, 62, 102031.

[16] Smarr, B. L., Aschbacher, K., Fisher, S. M., Chowdhary, A., Dilchert, S., Puldon, K., ... & Mason, A. E. (2020). Feasibility of continuous fever monitoring using wearable devices. Scientific reports, 10(1), 1-11.

[17]Agarwal, P., & Kumar, S. (2022). Electroencephalography-based imagined speech recognition using deep long short-term memory network. ETRI Journal, 44(4), 672-685.

[18]Davila, C. E., Wang, D. X., Ritzer, M., Moran, R., & Lega, B. C. (2022). A Control-Theoretical System for Modulating Hippocampal Gamma Oscillations Using Stimulation of the Posterior Cingulate Cortex. IEEE Transactions on Neural Systems and Rehabilitation Engineering, 30, 2242-2253.

[19] Gupta, K., Bajaj, V., & Ansari, I. A. (2022). A support system for automatic classification of hypertension using BCG signals. Expert Systems with Applications, 119058.

[20] M. R. Carlos and L. C. González and J. Wahlström and R. Cornejo and F. Martínez, "Becoming smarter at characterizing potholes and speed bumps from smartphone data - Introducing a second-generation inference problem," in IEEE Transactions on Mobile Computing., , . doi: 10.1109/TMC.2019.2947443

[21] Zhuang, F., Qi, Z., Duan, K., Xi, D., Zhu, Y., Zhu, H., ... & He, Q. (2020). A comprehensive survey on transfer learning. Proceedings of the IEEE, 109(1), 43-76.

[22] Yang, Q., Zhou, S.s., Wang, P., Zhang, J., 2021. Application of signal processing and support vector machine to transverse cracking detection in asphalt pavement. Journal of Central South University 28, 2451– 2462.

[23] Martinez-Ríos, E. A., Bustamante-Bello, R., & Navarro-Tuch, S. A. (2023). Generalized Morse Wavelets parameter selection and transfer learning for pavement transverse cracking detection. Engineering Applications of Artificial Intelligence, 123, 106355.

Thanks for your attention and time.

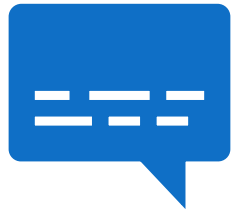

Questions, comments, or suggestions?

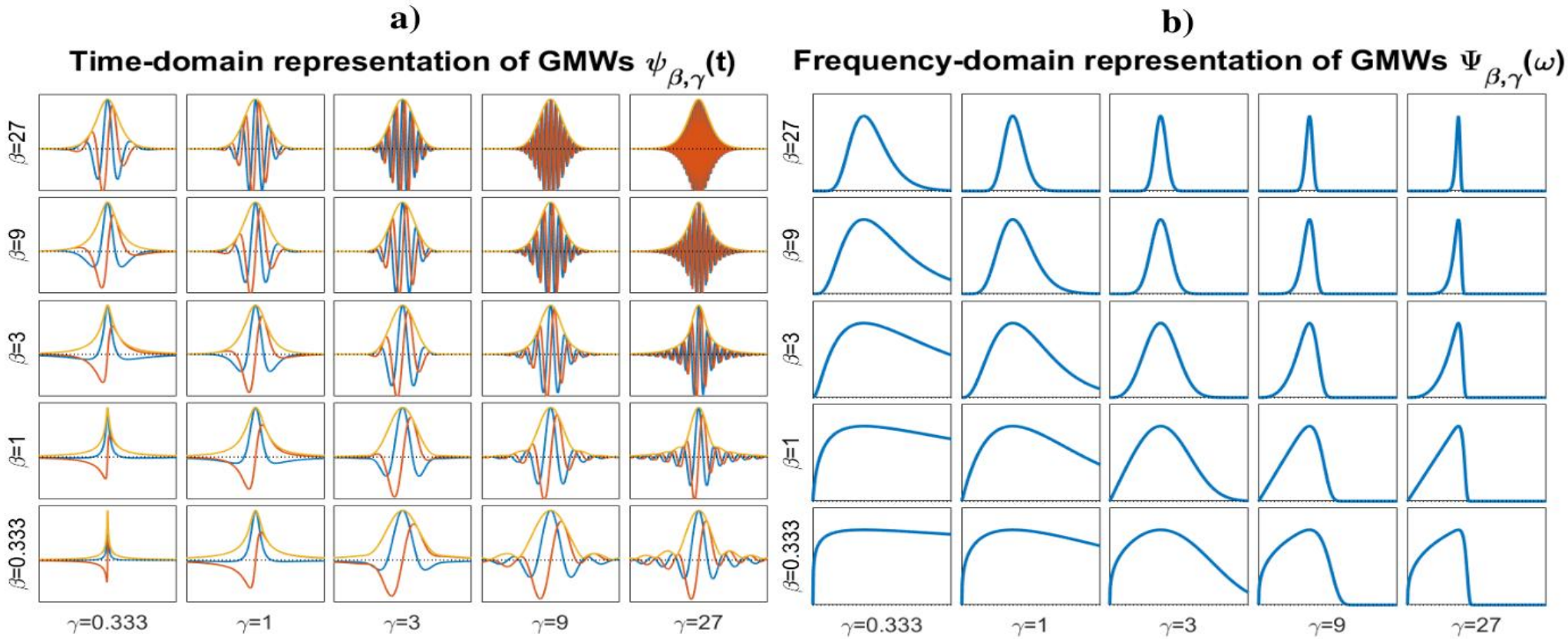

Selection of Gamma and Beta

Figure . Time-domain representation (left) and Frequency-domain representation (right) of the generalized morse wavelet for different values of gamma and beta.

Tecnológico de Monterrey

Parametrizations of gamma and beta.

Table . Parametrizations of generalized morse wavelets used in the literature.

Author	Gamma and beta values	Signal type	Application
Wachowiak et al. [14]	$\gamma = 3$ $\beta = 4$ $(P^2 = 12)$	ECG data	Assessing of heart variability through ECG
Cartas-Rosado et al. [15]	$\gamma = 3$ $P^2 = 60$ $(\beta = 20)$	ECG data	Analysis of heart rate variability and estimation of the automatic cardiac regulation.
Smarr et al. [16]	$\gamma = 3$ $\beta = 5$ $(P^2 = 15)$	Temperature time series data	Analyze temperature data through the CWT.
Agarwal et al. [17]	**Not reported**	EEG data	Imagined speech recognition performed through CWT and CNN
Davila et al. [18]	$\gamma = 3$ $P^2 = 60$ $(\beta = 20)$	EEG data	Estimation of the root-mean-square gamma power through a CWT filter-bank

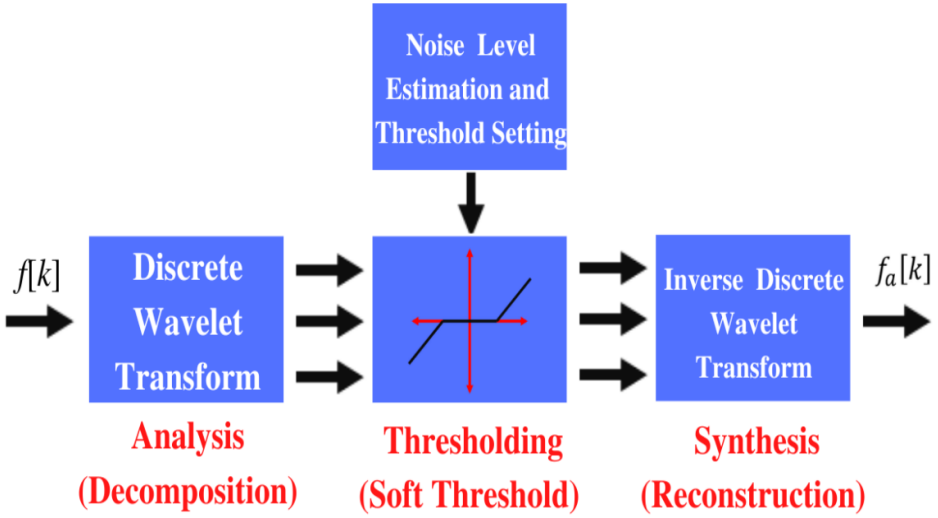

Figure . Procedure for applying wavelet de-noising.

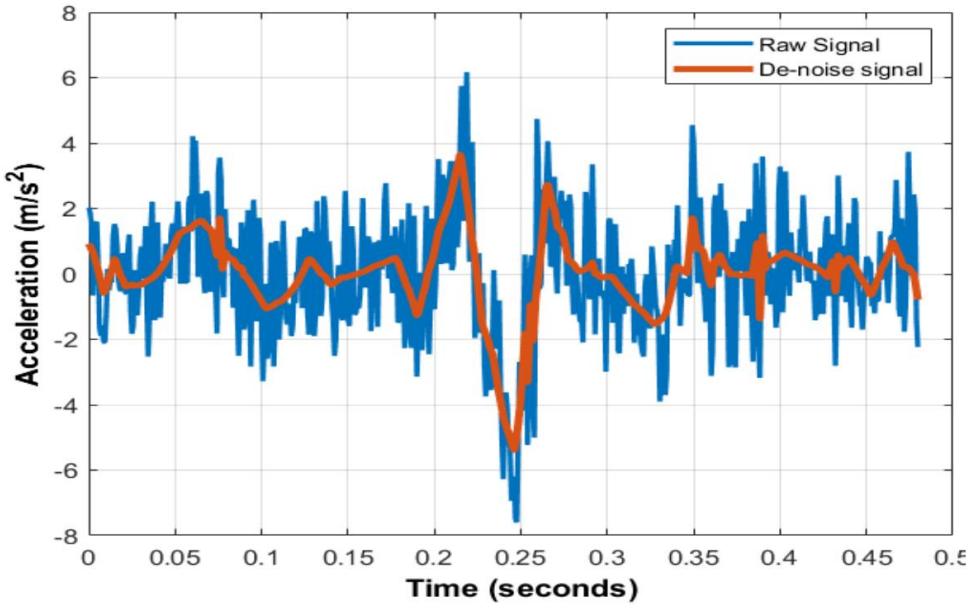

Figure . Comparison of raw accelerometer data with the filter version.

Tecnológico de Monterrey

Pre-processing steps

Noise estimation technique: Universal Thresholding.

Thresholding rule: soft thresholding.

Wavelet: Symlet order 3.

Decomposition Level: 4.

Parametrization based on the work of Yang et al.

Tecnológico de Monterrey

Table . Minimum ARMSE for each curve of voices per octave [23].

Voices per Octave	Time-Bandwidth Product (P^2)	Beta (β)	ARMSE	Reconstruction Mean Squared Errors Outliers	Reconstruction Mean Squared Errors Percentage of Outliers	Log Reconstruction Mean Squared Errors Outliers	Log Reconstruction Mean Squared Errors Percentage of Outliers
1	4	1.3333	0.0037	28	8.5627	1	0.3058
2	4	1.3333	0.0041	31	9.4801	3	0.9174
3	5	1.6667	0.0044	21	6.4220	3	0.9174
4	4	1.3333	0.0049	31	9.4801	4	1.2232
5	5	1.6667	0.0052	26	7.9511	4	1.2232
6	4	1.3333	0.0056	31	9.4801	4	1.2232
7	4	1.3333	0.0057	32	9.7859	3	0.9174
8	4	1.3333	0.0057	28	8.5627	4	1.2232
9	4	1.3333	0.0057	30	9.1743	4	1.2232
10	4	1.3333	0.0060	31	9.4801	4	1.2232

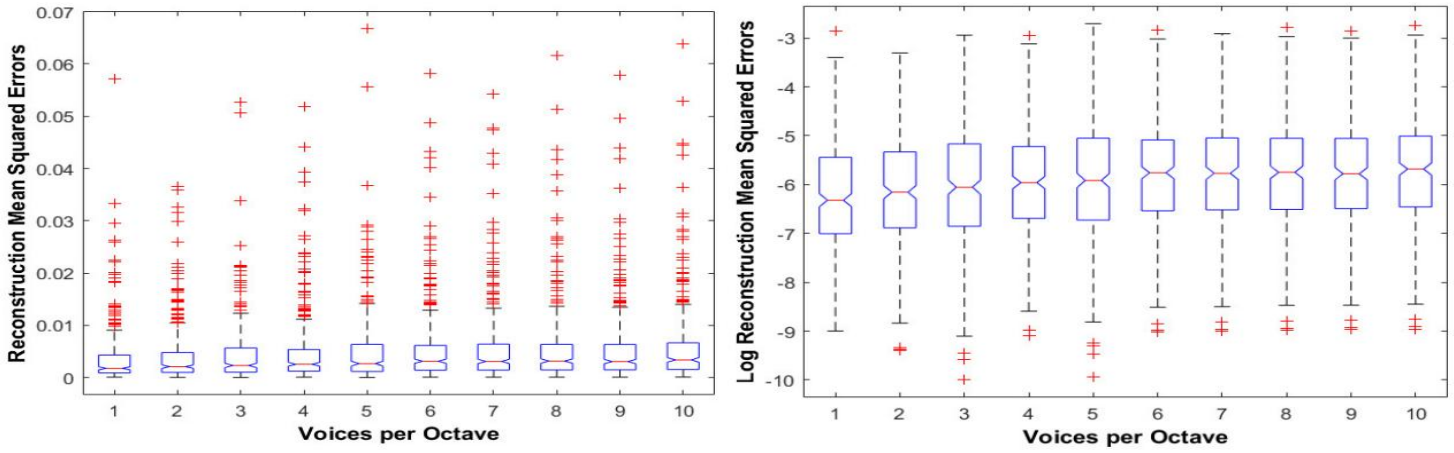

(a) (b)

Figure . Box plots of the Reconstruction Mean Square Error that produce the minimum ARMSE for each value of voices per octave [23].

Table . Results of the Shapiro-Wilk test and Barlett's of the Log Reconstruction Mean Squared errors distribution [23].

Shapiro-Wilk Test		
$\alpha = 0.05$		
Voices Per Octave	Test Statistic	p-value
1	0.9956	0.4881
2	0.9968	0.7727
3	0.9941	0.2089
4	0.9973	0.8615
5	0.9950	0.3171
6	0.9975	0.9008
7	0.9973	0.8729
8	0.9976	0.9226
9	0.9972	0.8594
10	0.9977	0.9309

Bartlett's Test			
$\alpha = 0.05$			
Voices per Octave	Count	Mean	Standard Deviation
1	327	-6.2276	1.10197
2	327	-6.1367	1.1574
3	327	-6.0692	1.20191
4	327	-5.938	1.12364
5	327	-5.944	1.22733
6	327	-5.793	1.12202
7	327	-5.7832	1.12797
8	327	-5.7821	1.11612
9	327	-5.7775	1.11771
10	327	-5.7273	1.11742
Pooled	3270	-5.9179	1.14203
Bartlett's statistic		7.646	
Degrees of Freedom		9	
p-value		0.5700	

Table One-Way ANOVA results and multiple comparisons test.

One-Way ANOVA ($\alpha = 0.05$)					
Source of Variation	Sum of Squares	Degrees of Freedom	Mean of Squares	F-Statistic	p-value
Between Groups	90.25	9	10.0275	7.69	$\mathbf{2.93454^{-11}}$
Within Groups	4251.77	3260	1.3042		
Total	4342.02	3269	Not Applicable		

Multiple comparisons test					
Group A (Voices)	Group B (Voices)	Lower Limit	A-B	Upper Limit	p-value
1	2	-0.37344	-0.090878	0.19168	0.9913
1	3	-0.44097	-0.15841	0.12415	0.75204
1	4	-0.57219	-0.28963	-0.0070682	0.039219
1	5	-0.56611	-0.28355	-0.00098642	0.048358
1	6	-0.71717	-0.43461	-0.15205	$\mathbf{4.9744^{-5}}$
1	7	-0.72692	-0.44436	-0.1618	$\mathbf{2.858^{-5}}$
1	8	-0.72805	-0.44549	-0.16293	$\mathbf{2.6783^{-5}}$
1	9	-0.73261	-0.45005	-0.16749	$\mathbf{2.0571^{-5}}$
1	10	-0.78289	-0.50033	-0.21777	$\mathbf{9.3017^{-7}}$
2	3	-0.3501	-0.067536	0.21502	0.99911

Bonferroni correction.
(Reduce the Type 1 error)

$$\alpha = \frac{0.05}{45} = 0.0011$$

Table One-Way ANOVA results and multiple comparisons test.

2	4	-0.48131	-0.19875	0.083809	0.43913
2	5	-0.47523	-0.19267	0.089891	0.48668
2	6	-0.62629	-0.34373	-0.061173	0.0046668
2	7	-0.63605	-0.35349	-0.070927	0.0030306
2	8	-0.63718	-0.35462	-0.072056	0.0028804
2	9	-0.64173	-0.35917	-0.076612	0.0023414
2	10	-0.69201	-0.40945	-0.12689	**0.00019594**
3	4	-0.41377	-0.13121	0.15135	0.90441
3	5	-0.40769	0.12513	0.15743	0.92732
3	6	-0.55876	-0.2762	0.006363	0.061761
3	7	-0.56851	-0.28595	-0.0033912	0.044548
3	8	-0.56964	-0.28708	-0.0045195	0.04285
3	9	-0.5742	-0.29164	-0.0090757	0.036548
3	10	-0.62447	-0.34191	-0.059354	0.0050503
4	5	-0.27648	0.0060818	0.28864	1
4	6	-0.42754	-0.14498	0.13758	0.83708
4	7	-0.4373	-0.15474	0.12782	0.77701
4	8	-0.43842	-0.15587	0.12669	0.76947
4	9	-0.44298	-0.16042	0.12214	0.73793
4	10	-0.49326	-0.2107	0.071861	0.3508
5	6	-0.43362	-0.15106	0.1315	0.80074
5	7	-0.44338	-0.16082	0.12174	0.73511
5	8	-0.44451	-0.16195	0.12061	0.72701
5	9	-0.44906	-0.1665	0.11606	0.69343
5	10	-0.49934	-0.21678	0.065779	0.30936
6	7	-0.29231	-0.0097542	0.27281	1
6	8	-0.29344	-0.010883	0.27168	1
6	9	-0.298	-0.015439	0.26712	1
6	10	-0.34828	-0.065717	0.21684	0.99928
7	8	-0.28369	-0.0011284	0.28143	1
7	9	-0.28824	-0.0056845	0.27688	1
7	10	-0.33852	-0.055963	0.2266	0.99981
8	9	-0.28712	-0.0045562	0.278	1
8	10	-0.33739	-0.054834	0.22773	0.99984
9	10	-0.33284	-0.050278	0.23228	0.99992

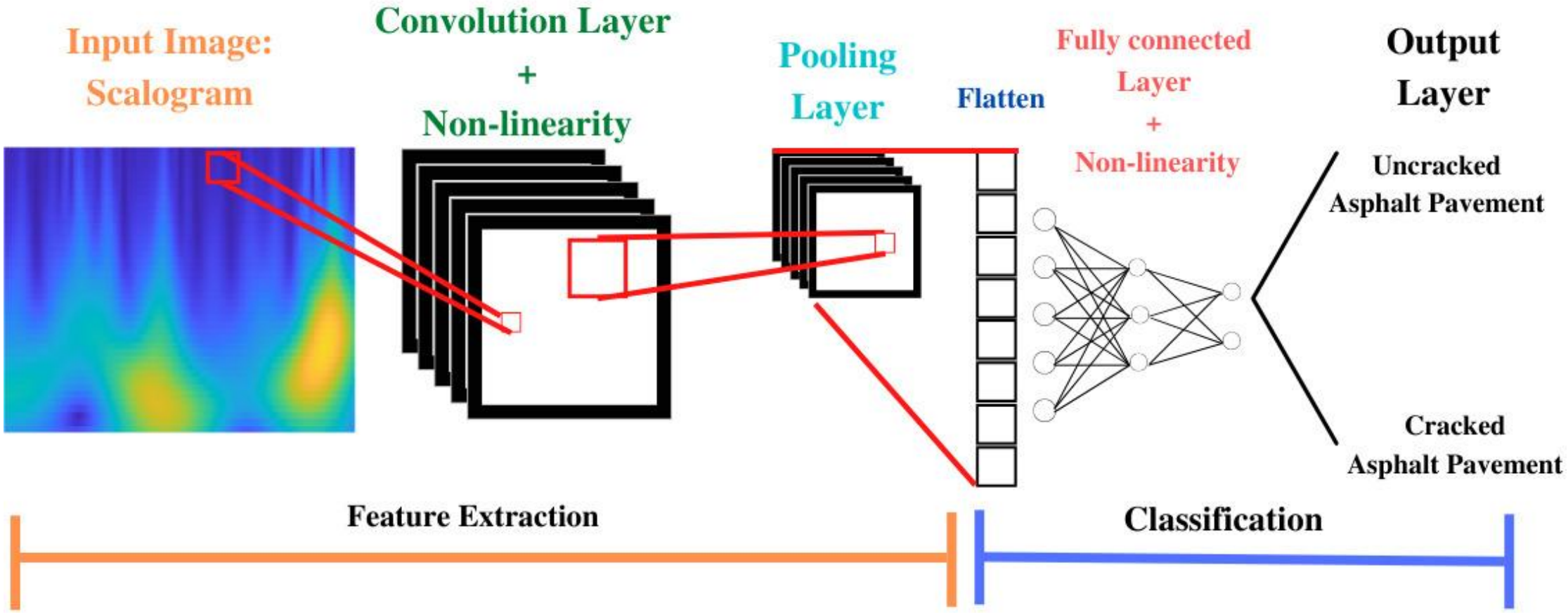

Figure Convolutional neural Network Overview [23].

Transfer Learning

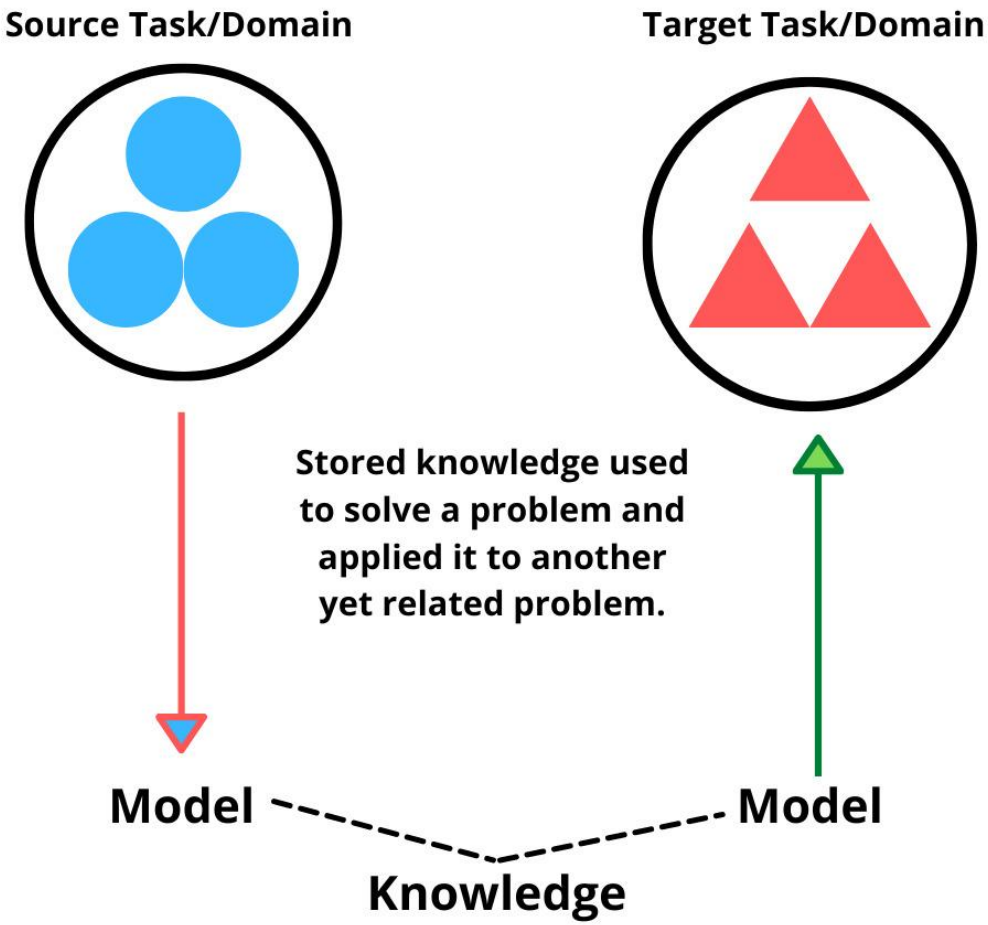

Figure. Transfer Learning Overview [23].

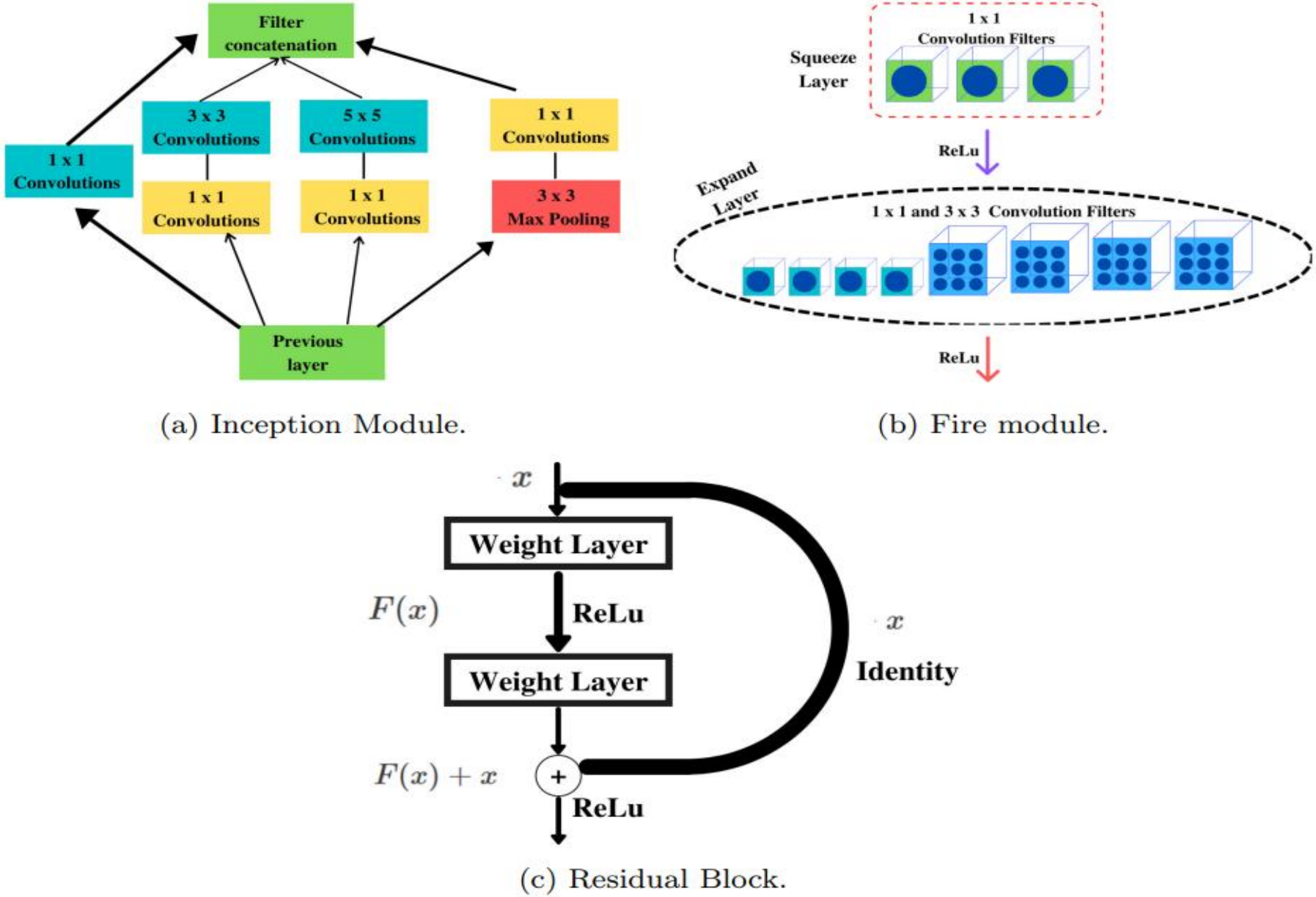

Figure Pre-trained convolutional neural networks modules [23].

Results of GoogLeNet

Table 4. Performance of the GoogLeNet [23].

Fold	Training Accuraccy %	Accuracy %	Sensitivity %	Specificity %	Precision %	NPV %	F1-Score %	AUC	Time
1	99.2337	81.8182	77.2727	84.0909	70.8333	88.0952	73.9130	0.9236	6 min 16 sec
2	100	95.3846	90.9091	97.6744	95.2381	95.4545	93.0233	0.9757	5 min 59 sec
3	100	86.1538	66.6667	95.4545	87.5000	85.7143	75.6757	0.9318	5 min 57 sec
4	99.2366	87.6923	72.7273	95.3488	88.8889	87.2340	80.0000	0.9598	6 min 1 sec
5	96.5517	89.3939	77.2727	95.4545	89.4737	89.3617	82.9268	0.9669	5 min 51 sec
Average ± Standard Deviation	99.0044 ± 1.4234	88.0886 ± 4.9536	**76.9697 ± 8.9253**	**93.6047 ± 5.4074**	86.3868 ± 9.1827	89.1720 ± 3.7542	81.1078 ± 7.5463	**0.9516 ± 0.0227**	6.0133 min ± 0.1547 min

Results of SqueezeNet

Table 5. Performance of the SqueezeNet [23].

Fold	Training Accuracy %	Accuracy %	Sensitivity %	Specificity %	Precision %	NPV %	F1-Score %	AUC %	Time
1	99.2337	84.8485	90.9091	81.8182	71.4286	94.7368	80.0000	0.9256	2 min 25 sec
2	99.2366	93.8462	86.3636	97.6744	95.0000	93.3333	90.4762	0.9556	2 min 42 sec
3	100.0000	90.7692	76.1905	97.7273	94.1176	89.5833	84.2105	0.9297	2 min 44 sec
4	98.4733	92.3077	81.8182	97.6744	94.7368	91.3043	87.8049	0.9799	2 min 43 sec
5	100.0000	87.8788	86.3636	88.6364	79.1667	92.8571	82.6087	0.9576	2 min 42 sec
Average ± Standard Deviation	99.3887 ± 0.6388	89.9301 ± 3.5959	**84.3290 ± 5.5704**	**92.7061 ± 7.2403**	86.8899 ± 10.9349	92.3630 ± 1.9792	85.0201 ± 4.1592	**0.9497 ± 0.0223**	2.6533 min ± 0.1330 min

Results of ResNet18

Table 6. Performance of the ResNet18 [23].

Fold	Training Accuracy %	Accuracy %	Sensitivity %	Specificity %	Precision %	NPV %	F1-Score %	AUC	Time
1	98.8506	86.3636	72.7273	93.1818	84.2105	87.2340	78.0488	0.9174	6 min 16 sec
2	99.6183	92.3077	81.8182	97.6744	84.2105	91.3043	87.8049	0.9672	5 min 30 sec
3	99.6183	90.7692	71.4286	100.0000	100.0000	88.0000	83.3333	0.9091	5 min 17 sec
4	99.6183	93.8462	81.8182	100.0000	100.0000	91.4894	90.0000	0.9493	5 min 25 sec
5	99.6169	92.4242	81.8182	97.7273	94.7368	91.4894	87.8049	0.9493	6 min 9 sec
Average ± Standard Deviation	99.4645 ± 0.3432	91.1422 ± 2.8848	**77.9221 ± 5.3547**	**97.7167 ± 2.7836**	94.7368 ± 6.4460	89.9034 ± 2.1060	85.3984 ± 4.7707	**0.9391 ± 0.0247**	5.7233 min ± 0.4513 min

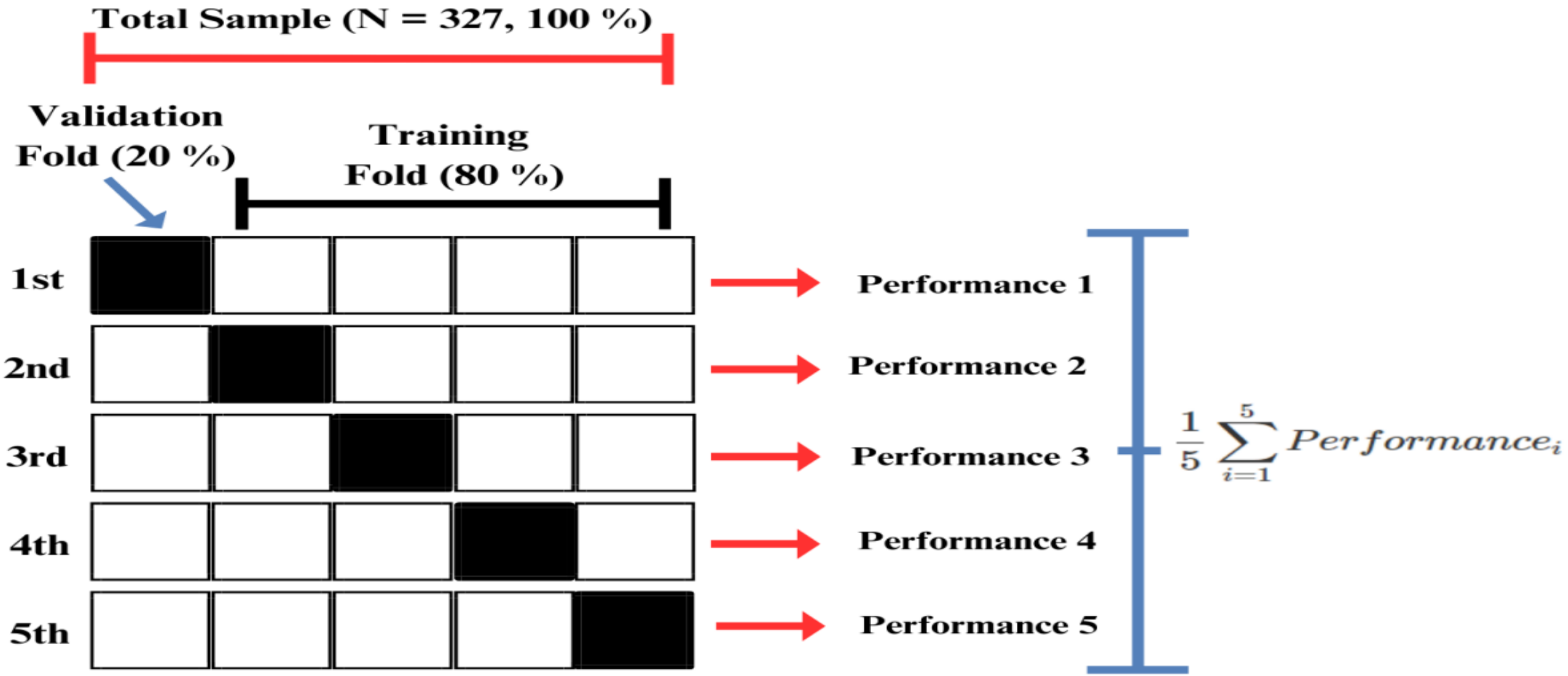

Figure . 5-fold cross-validation used to measure the generalization performance od the proposed CNNs [23].

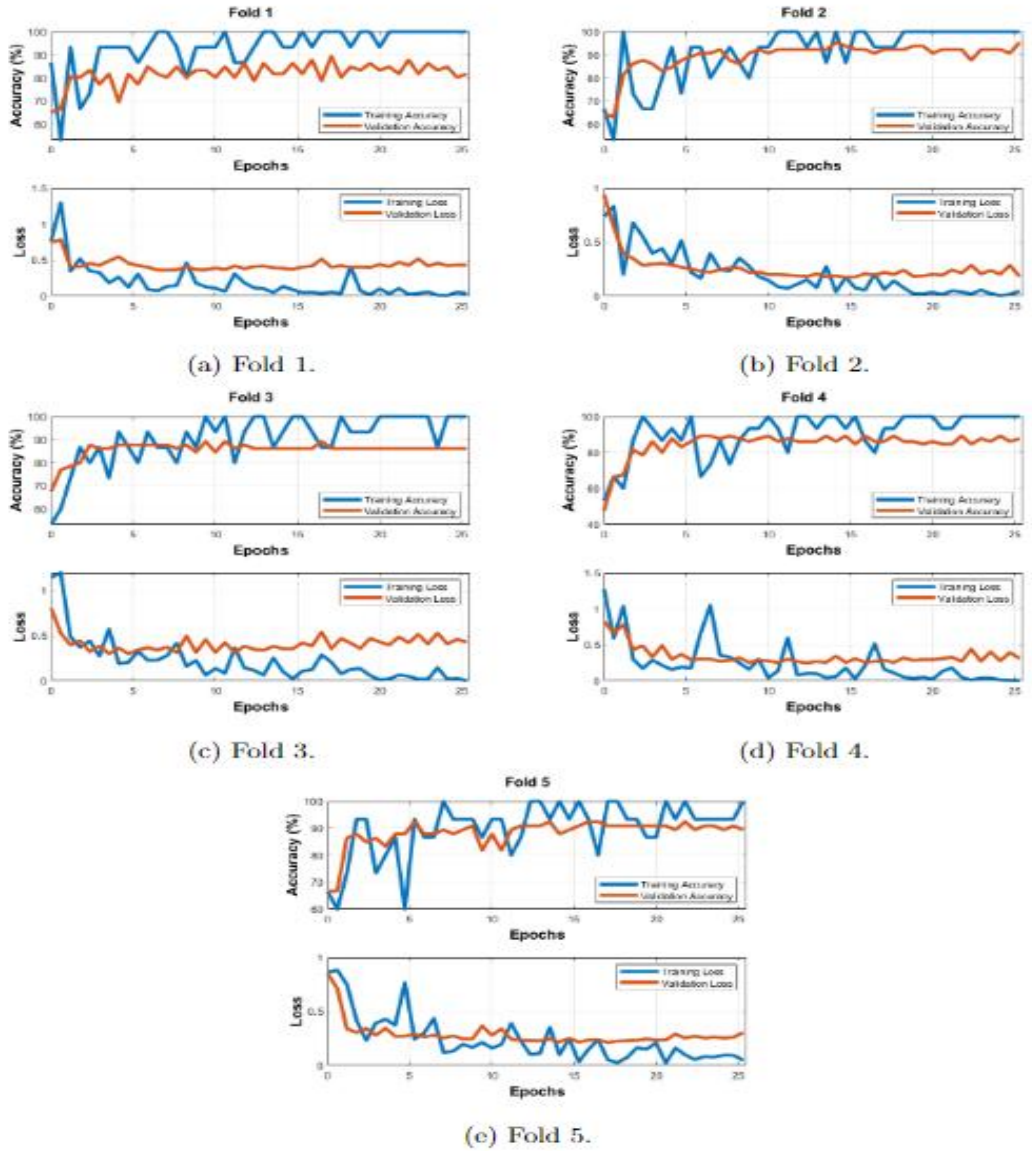

(a) Fold 1. (b) Fold 2. (c) Fold 3. (d) Fold 4. (e) Fold 5.

Figure Learning curves of GoogLeNet [23].

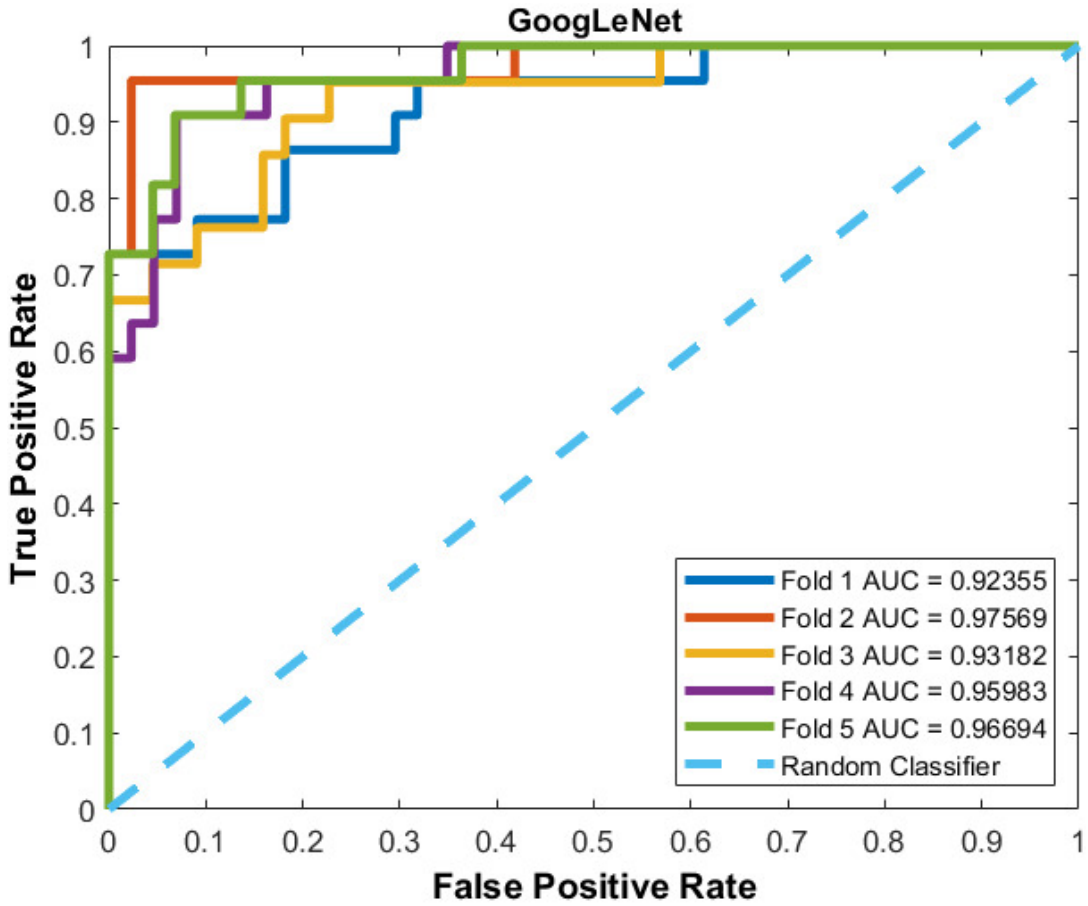

Figure ROCs Curves of GoogLeNet [23].

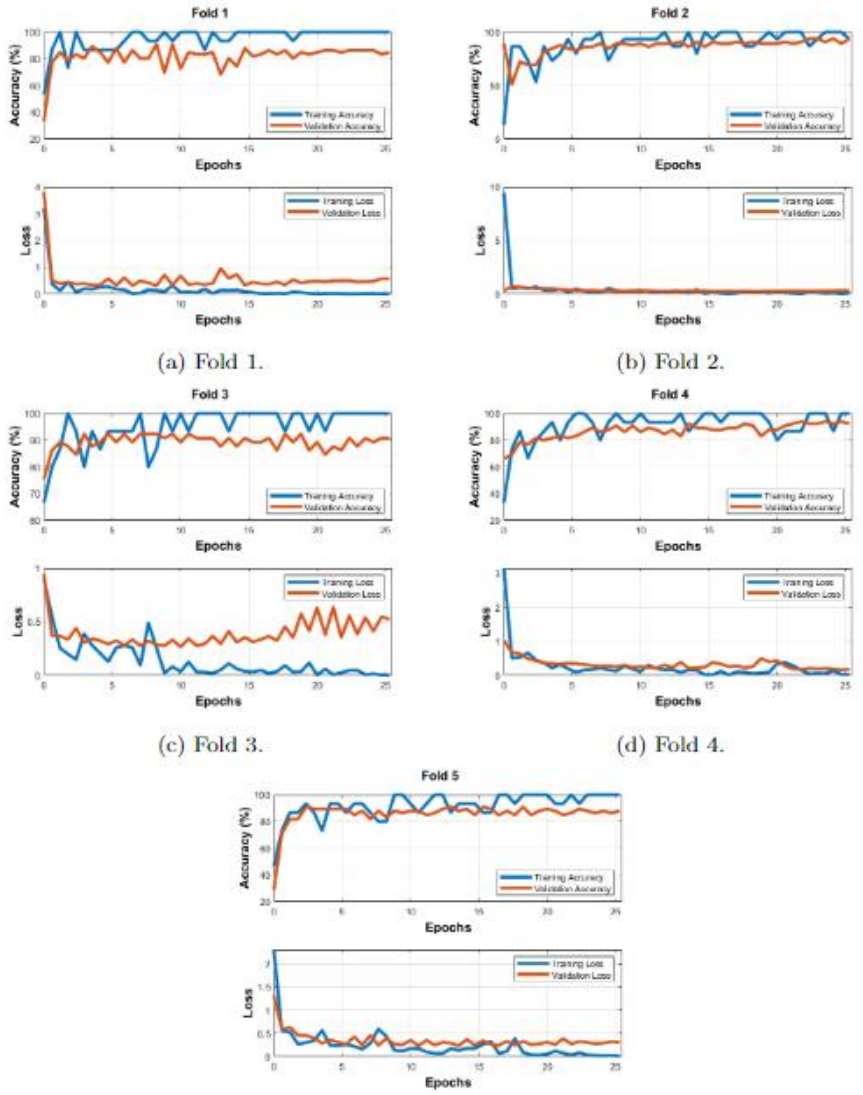

(a) Fold 1. (b) Fold 2. (c) Fold 3. (d) Fold 4. (e) Fold 5.

Figure Learning curves of SqueezeNet [23].

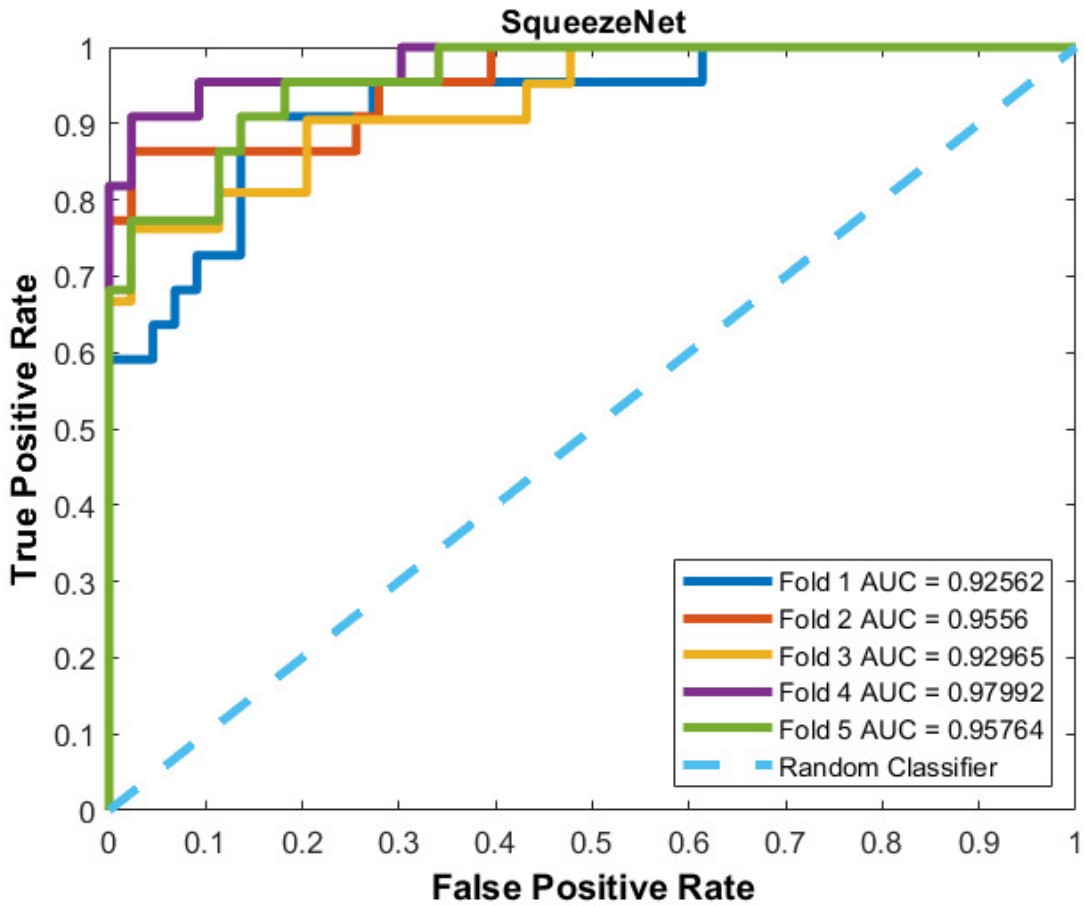

Figure ROCs Curves of SqueezeNet [23].

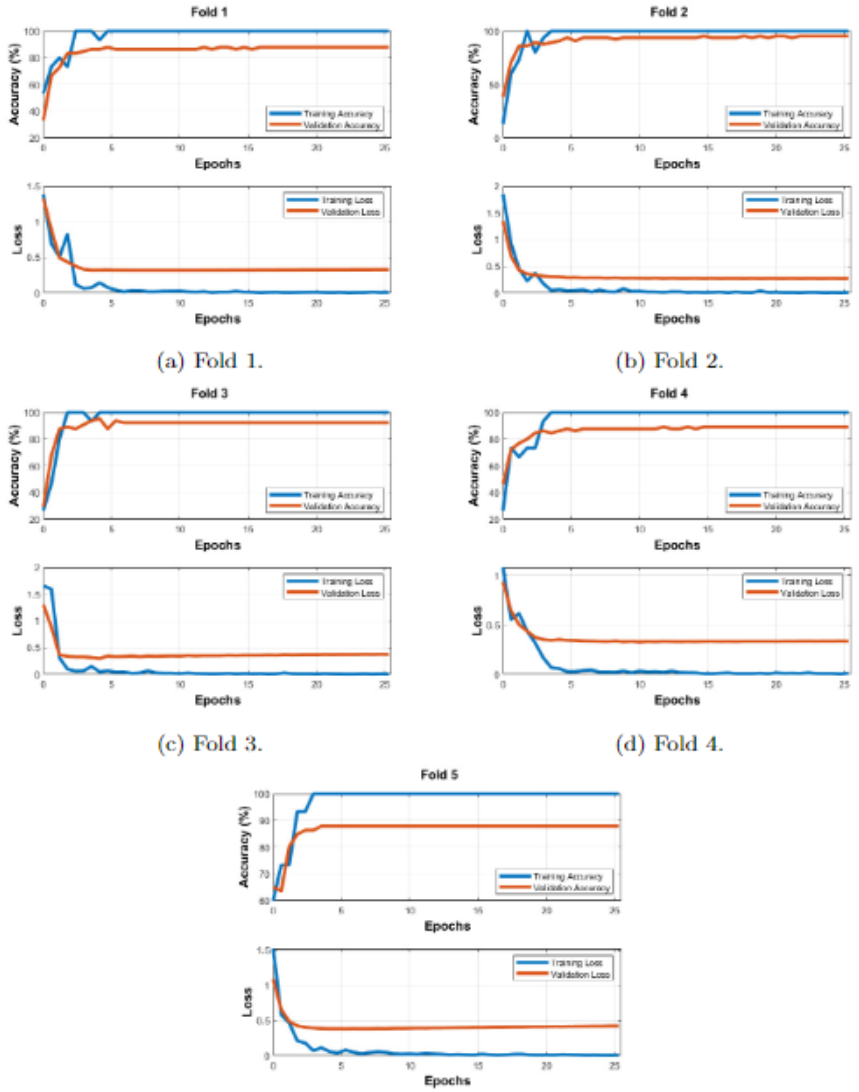

(a) Fold 1. (b) Fold 2. (c) Fold 3. (d) Fold 4. (e) Fold 5.

Figure Learning curves of ResNet18 [23].

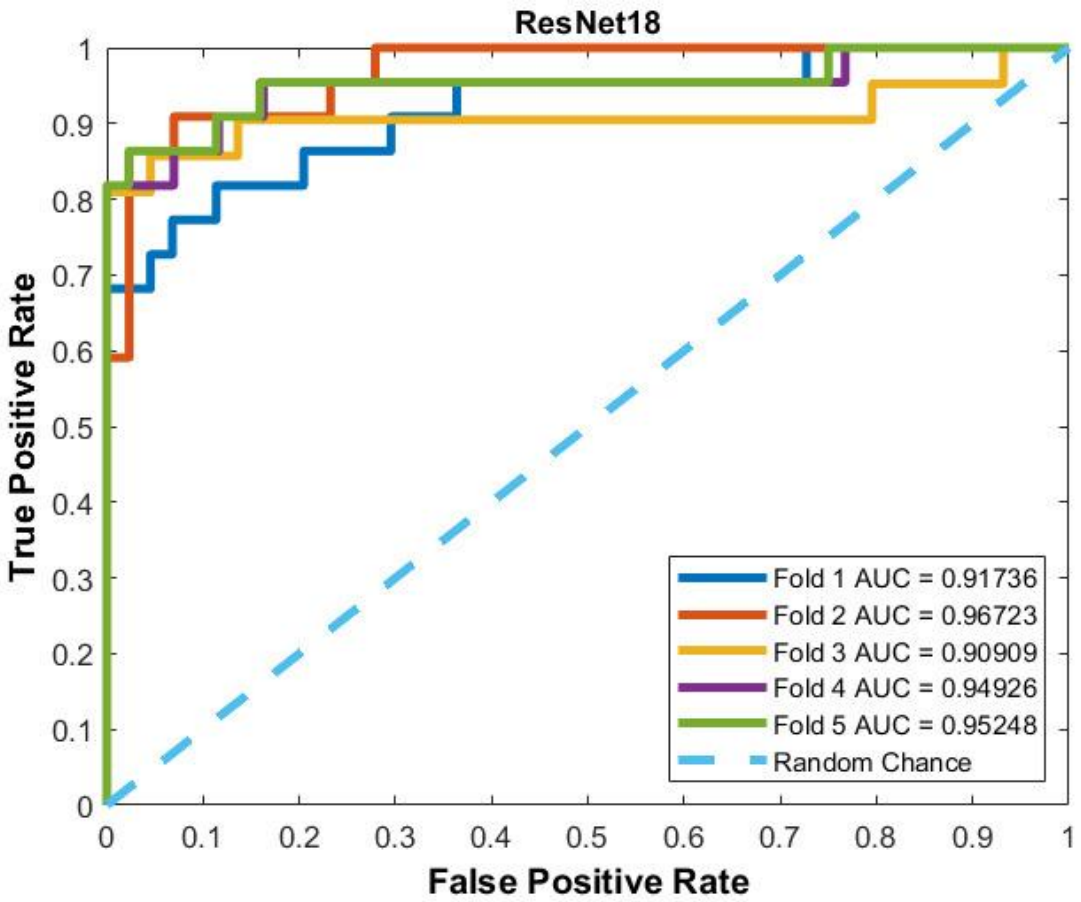

Figure ROCs Curves of ResNet18 [23].

Figure 20. ROCs Curves of GoogLeNet.

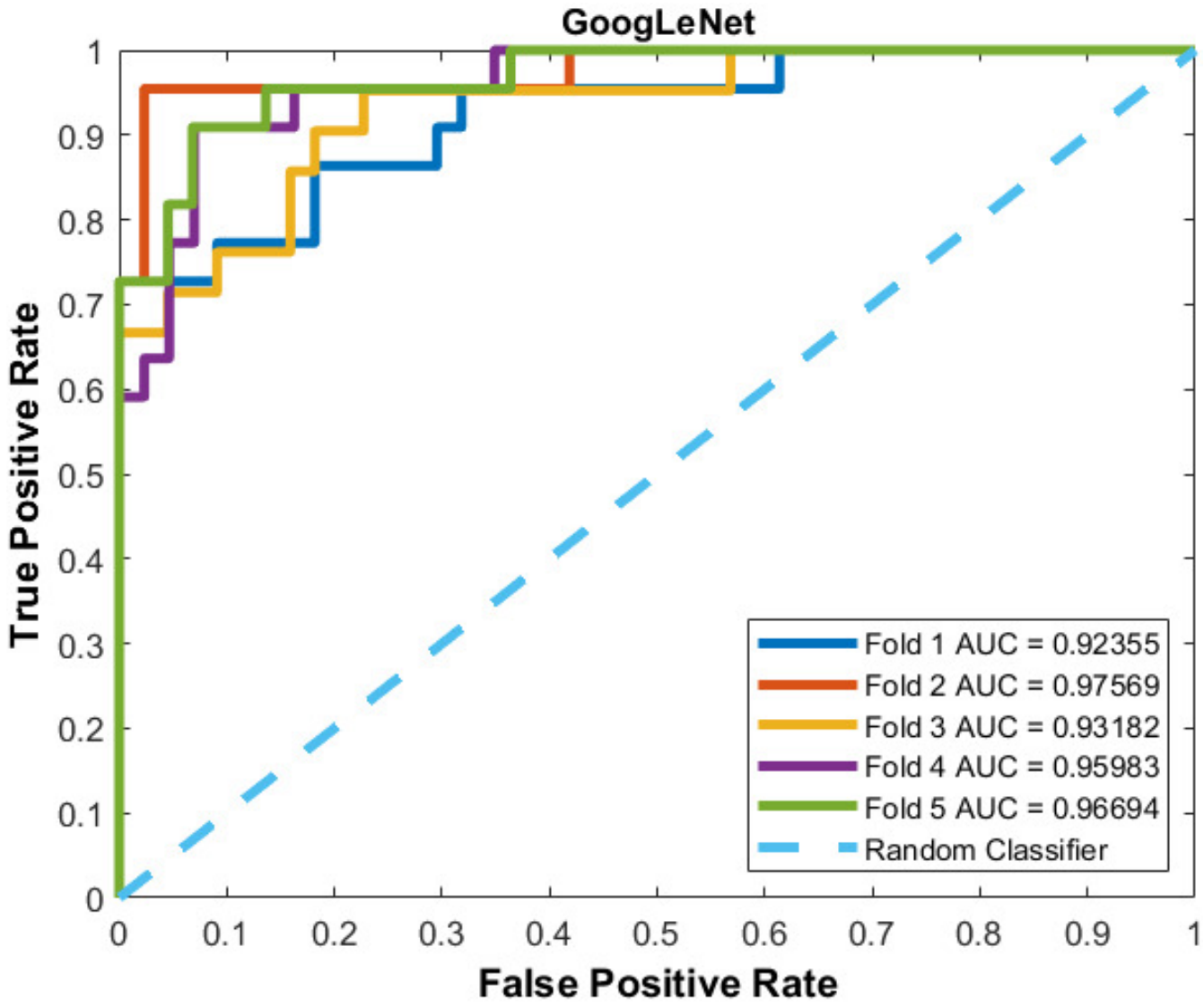

Figure ROCs Curves of SqueezeNet.

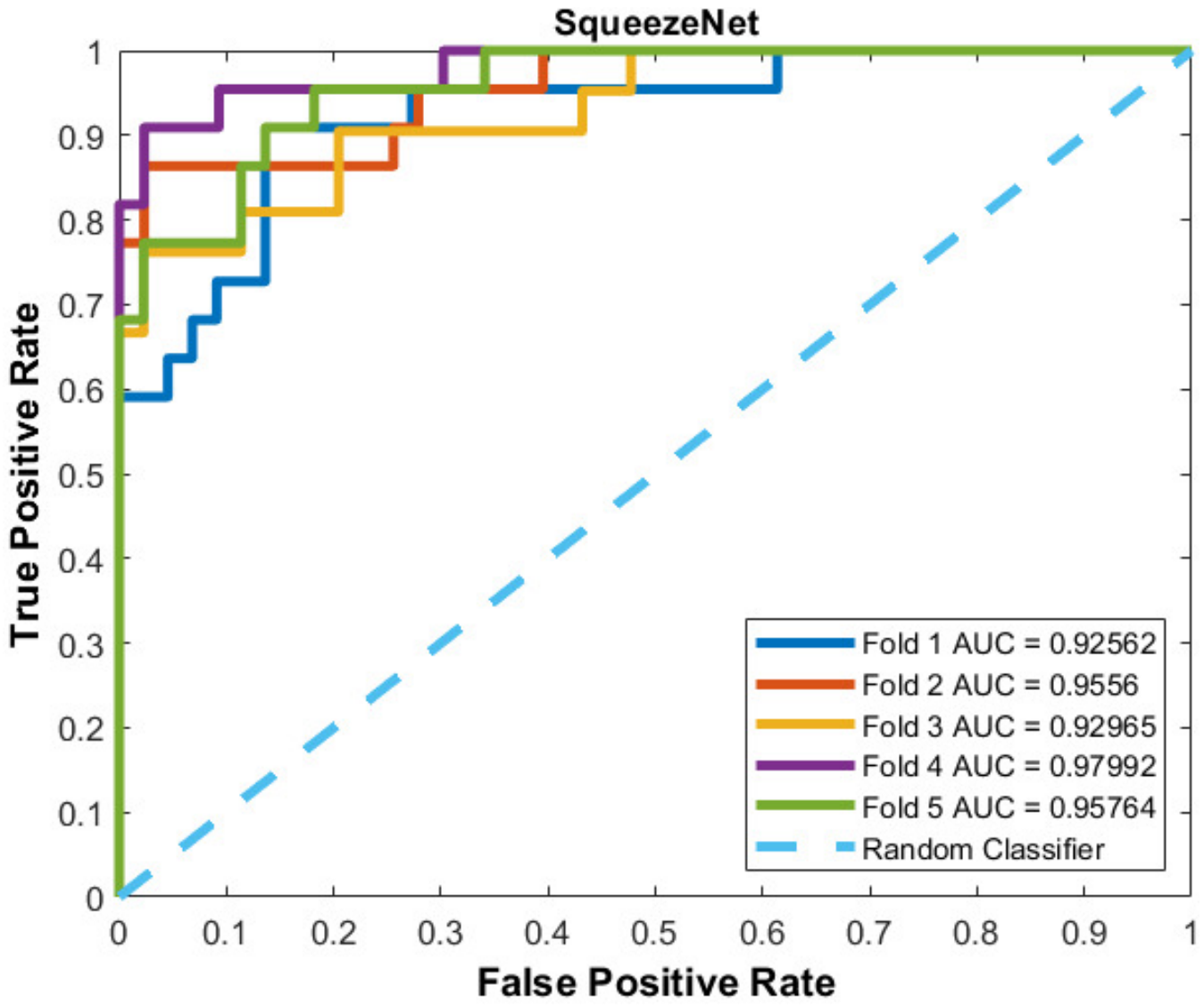

Tecnológico de Monterrey

Figure ROCs Curves of ResNet18.